Journal of Vibration Engineering & Technologies (2024) 12:7065–7097
https://doi.org/10.1007/s42417-023-01029-w

ORIGINAL PAPER

Realistic Modelling for Analysis of Train-Structure and Ballasted-Track Interaction for High-Speed Trains

Mustafa Eroğlu[1] · Mehmet Akif Koç[2] · İsmail Esen[3] · Recep Kozan[1]

Received: 17 March 2023 / Revised: 10 May 2023 / Accepted: 20 May 2023 / Published online: 26 June 2023

Abstract
Purpose In this study, a new train-track-bridge interaction system (TTBIS) is modelled, and the interaction of the system is analysed to calculate the dynamic responses of the (TTBIS). Considering the lateral and vertical dynamic movements, the entire train is realistically modelled with 31 degrees of freedom.
Methods The track system is realistically modelled as flexible rail, and the infrastructure system supporting the rail with eight parameters. So, the track system consists of flexible rail, two parameter rail pad, sleeper, ballast parameters. The bridge was modelled using thin beam theory and integrated motion equation was obtained using the Lagrange method.
The analytical solution of motion equation was conducted by setting up an algorithm using the Runge–Kutta method with a specially written code.
Results As a result of the analyses made, the length of the bridge is 50 m or less, which does not affect the vertical movements of the train. In addition, Thanks to the track system, the dynamic responses affecting the train have been reduced. It is also understood that the vertical dynamic behavior of the train is a minimum in every four wagons.
Conclusion As the significance of this research, it was seen that bridge flexibility, natural vibration frequency, track parameters, travel speed, and the number of wagons have essential effects in terms of safe travel of high-speed-train.

Keywords Train-track-bridge interaction · High-speed train · Full train model · Runge–Kutta method

Introduction

Background

As a result of the increase in economic and safe transportation demands, high-speed train transportation has become a critical alternative today and the physical infrastructure of transportation and the physical structure of the train system have become an important research topic in engineering. As transportation speeds increase, it is a vital issue in terms of travel safety that engineering calculations are made with remarkably high precision in accordance with real physical conditions, and the design and development of a train suspension system and track infrastructure system suitable for the conditions. The rail system on which the train passes and in some cases the bridge systems over which it passes are flexible systems.

Formulation of the Problem of Interest for this Investigation and Literature Survey

Trains are produced with suspension systems in terms of travel comfort and transportation safety. Due to these facts, the train dynamically interacts with the track and bridge while in motion or when crossing the bridge [1, 2]. In this context, Tiwari et al. examined the ride quality and comfort of a railway vehicle that used a secondary suspension system based on insulators and a laminated rubber base [3]. Sabaa et al. examined vibrational movements for transportation devices used in daily life and evaluated them in terms of resonance [4]. In the literature, train-bridge interactions have been studied with simple models without considering the rail effect. When the results of the literature studies are

✉ Mustafa Eroğlu
mustafaeroglu@sakarya.edu.tr

1 Engineering Faculty, Mechanical Engineering Department, Sakarya University, 54187 Sakarya, Turkey

2 Technology Faculty, Mechatronics Engineering Department, Sakarya University of Applied Sciences, 54187 Sakarya, Turkey

3 Engineering Faculty, Mechanical Engineering Department, Karabük University, 78050 Karabük, Turkey

examined, it is understood that the flexibility of the bridge and the parameters of the train suspension system are effective in the train-bridge interaction [5]. In addition, it significantly affects driving safety in high-speed trains exposed to strong winds. Li et al. investigated the vibrational dynamics of wheel-rail collisions for high-speed trains operating in crosswinds [6]. Liu et al. concentrated on the crosswind phenomenon to better understand the occurrence of a train derailment [7]. Liu et al. investigate how crosswind affects the train-rail-bridge system's dynamic responses [8].

The moving load is generally examined in three categories as concentrated force, moving mass and sprung mass. Train track and bridge interaction subject is within the scope of moving load in the scientific literature, and the first studies on this subject are simplified model studies involving the interaction of a concentrated force with a flexible structure while it passes over a flexible structure [9–14]. Jiang et al. investigated the dynamic responses of a multilayer beam structure system on a railway track under a moving load [15]. Moving mass studies take into account the inertial effects of the load's mass and the effects of the centrifugal force, and Coriolis force, which are the interaction forces of the mass with the deformed beam [16–26]. Studies examining the moving load problem as a sprung mass are studies that only consider the interaction force arising from the vibration acceleration of the mass on the beam as the contact force, without considering the Coriolis and centrifugal forces arising from the interaction of the mass with the beam [9, 27–29]. As a more advanced model, a two-axle vehicle-bridge model with 4-DOFs was presented by Fryba and Wen [9, 28]. When train subsystems consisting of a carriage, two bogies, and wheelsets are modeled together with the bridge girder, this model is called as train-bridge interaction (TBI) models in the literature. There are different simplified applications of TBI in the literature [24–27]. High speed train has not been conducted much in the literature, only 10 DOF train models are presented with simple assumptions in the study [30]. Studies consisting of two distinct subsystems, train and bridge, have been investigated and some of which are summarized above. However, in practice, there is a track system consisting of sleepers, rail pads, and ballast on the railway line. In this study, simulation software has been designed to find the dynamic responses of the train and bridge along with the track system, which is called the train-track-bridge interaction system (TTBIS). In fact, train, track, and bridge is a basic dynamic system combined with train-track and track-bridge. In other words, the track system creates a link between the bridge and the train [31]. In this study, the dynamic equations of the TTBIS model were solved by using Matlab software, which is mostly used in the literature [32]. The train, bogies, and wheels are built based on multibody dynamics, while the bridge and rail are modelled as a simplified beam, which is adopted in the literature based on such models as Euler–Bernoulli or Timoshenko beams. For example, Cheung et al. performed vibration analysis of multi-span uniform bridges, modelled according to the Euler–Bernoulli beam theorem, exposed to a moving vehicle with 2-DOFs [33]. With regard to the longitudinal track-structure interaction, Stollwitzer et al. concentrate on the experimental determination of the dynamic properties [34]. Lou et al. investigated the dynamic effect of vehicle, rail, and bridge by using two different track models. It is demonstrated that the dynamic reactions are influenced by the sleeper mass [35]. Kohl et al. investigated the dynamic vehicle-bridge interaction using a large dataset of approximately 100 bridge structures and 25 vehicles [36]. A semi-analytical method based on the lumped parameter model was presented by König et al. for the analysis of the dynamic interaction system between trains, rails, bridges, and subsoil [37]. Zhang et al. suggested a new method based on the adaptive sampling proxy model to improve the efficiency of the train-bridge system's random vibration analysis [38]. Euler–Bernoulli beams are preferred in long-span beams since shear deformation values are not very important [39]. Many studies also use Timoshenko beam theories to consider the shear deflection effect [40, 41]. For example, the vibration analysis of Timoshenko cracked beams was carried out by Heydari et al. using a continuous model. They stated that the Timoshenko beam is preferable in the case of short beams compared to the Euler–Bernoulli beam model [42]. Koç modelled a bridge exposed to vibrations of a high-speed train, modelled with 10-DOFs, using Timoshenko and Euler–Bernoulli beam theories, and compared the results in terms of bridge and train dynamics [43]. Similarly, Dixit conducted an analysis of damaged beams, using both beam theories and claimed that the Timoshenko beam theory is more effective than the Euler–Bernoulli beam theory in detecting small changes in the dynamic response of beams [44]. Investigating seismic effects is crucial when analyzing the dynamic responses of high-speed trains. In this context, the high-speed rail-bridge system's seismic response was estimated by Yu et al. [39]. By treating earthquake and road irregularity as random processes, Jin et al. used probability density development method to determine the probability density function of the wheel unloading extremes [40]. In the case of the Addis Ababa Light Rail Transit Service, Bizimungu and Nkundineza investigated the effect of track irregularities on rail vehicle vibration [45]. Vesali et al. experimented with the dynamic response of two-track multi-span railway bridges [46].

There are several methods for obtaining differential equations. By using mass, spring, and damping properties in Newton's second law [47] or D'Alembert's principle [48] with considering the specified forces, the equations of motion of elementary systems can be obtained. Systems with a single degree of freedom and systems having multiple mass, spring, and damper elements can be modelled by using the principle of virtual works [49]. On the other hand, the most commonly used method to obtain the multi-degree of freedom systems' motion equations is Lagrange's principle [50, 51] and Hamilton's principle [52], which can be classified as energy methods [53]. Rail and bridge element models are fourth-order partial differential equations, which can be transformed by Ritz's method into a second-order differential equation. [54] or Galerkin's method [55].

In train dynamics, either the normal mode superposition method [56–58] or the direct numerical integration method is preferred to solve equations of motion. In the direct numerical integration method, the equation of motion is solved by applying a step-by-step numerical procedure. In this method, time derivatives are usually approximated by using difference formulas [50] and can be solved with explicit methods such as fourth-order Runge–Kutta [59, 60] and Euler methods [61], and implicit methods such as Wilson θ [62] and Newmark β [63, 64].

The Novelty of this Study

In addition to the studies mentioned above, a comprehensive TTBIS simulation software has been developed in this paper. Thanks to TTBIS software, all factors affecting train dynamics can be considered. Studies in the literature do not compare the effect of the track while considered in a train-bridge coupled system. That is, there are no studies on how the track subsystem affects the train dynamics. Additionally, due to privacy and expertise concerns, the organizations likely to conduct this study don't provide their results. In the presented analysis results, the effects of with-track and without-track models on the results standing for the train and bridge dynamics are examined in detail. Moreover, the effect of the bridge length, track parameters and the velocity of train on the train dynamics was considered, which is found to be related with the concept of resonance. The track infrastructure is particularly important in terms of the dynamic interaction of the system, and quite simple models have been examined in the literature. In this study, a realistic track system is modelled, and the track system consists of a system with eight parameters following reality. So, the track system consists of independent parameters as flexible rail: flexural rigidity EI, unit mass μ_r, damping c_r; rail pad: stiffness k_p, damping c_p; sleeper: mass m_s, stiffness k_b, damping c_b; ballast: mass m_{ba}, stiffness k_f, damping c_f. Finally, three parameters for the rail, eight parameters for the sub-system supporting the rail, and a total of eleven parameter for the track system are considered. In addition, using the TTBIS software simulation developed in this study, a dynamic evaluation of the track-bridge subsystem can be made in case of multiple successive wagons. In other words, using the developed modelling, the bridge length, the effects of the train velocity, the train-track-bridge suspension parameter values, and even the multi-car and multi-bridge can be examined separately. The Lagrange equation has been used to generate the dynamic motion equation for the interaction of the bridge beam and the train. Using the state variables, the complete system's equation of motion was transformed into state-space form. An algorithm for the time domain using fourth-order Runge–Kutta is used in the suggested technique in this paper, which models both train dynamics and bridges and provides an accurate and quick solution procedure.

Organization of the Paper

The organization of this paper is divided into the following sections: In Sect. "Modeling of TTBIS", modeling of the train-track-bridge system is modeled. The numerical solution and validation of TTBi are conducted in Sect. "Numerical solution". In Sect. "Numerical analysis of full 3D high-speed TTBIS dynamics", extensive and comprehensive numerical results of the model discussed in this study are given. The main conclusion is presented in Sect. "Conclusions".

Modeling of TTBIS

In high-speed railway engineering, many different models have been preferred today to determine the dynamic behaviour of the train [31]. The railway bridges are modelled as simply supported beams, while trains are modelled as moving loads. TBI has been realized using moving load [9, 65, 66], moving mass [19, 26, 67], sprung mass [27], and suspended rigid beam models [12, 68] from the past to the present, respectively. With the development of technology and the widespread use of computer simulation software, two-dimensional (2D) [30, 69] and three-dimensional (3D) [70, 71] TBI models have also been improved.

In this paper, the TTBIS, illustrated in Fig. 1, has been considered to analyse the vertical and lateral dynamic responses of the train. TTBIS consists of three different subsystems as train, track, and bridge. While the train passes over the bridge at a specific speed, it vibrates the bridge and the track, which eventually affects the train dynamics and so reduces driving safety and passenger comfort.

Railway Car Model

Modelling of the High-Speed Train

The train model proposed in this study is shown schematically in Fig. 2. The examined vehicle model consists of a wagon moving at a constant speed, a bogie at the front and rear, and wheelsets, like many other models [70–73] studied before. Spring and damping elements are used to link components to one another. While a bogie and wheelset are connected by a primary suspension element, the bogie and wagon are connected by a secondary suspension element [69]. A 3D model was created to analyse the vertical and lateral vibrations of the train. Table 1 has the train parameters listed in Fig. 2. Also,

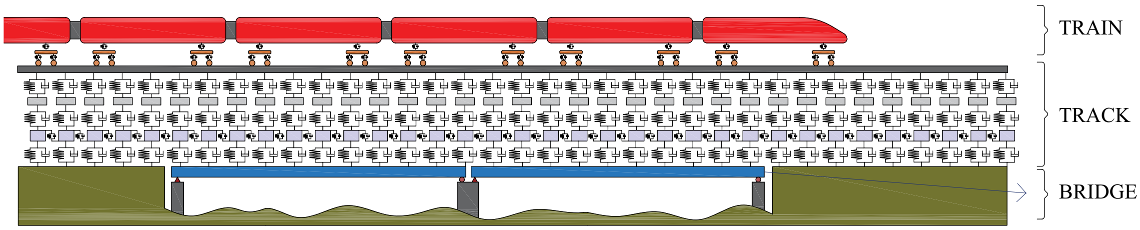

Fig. 1 The illustration of the train-track-bridge system model

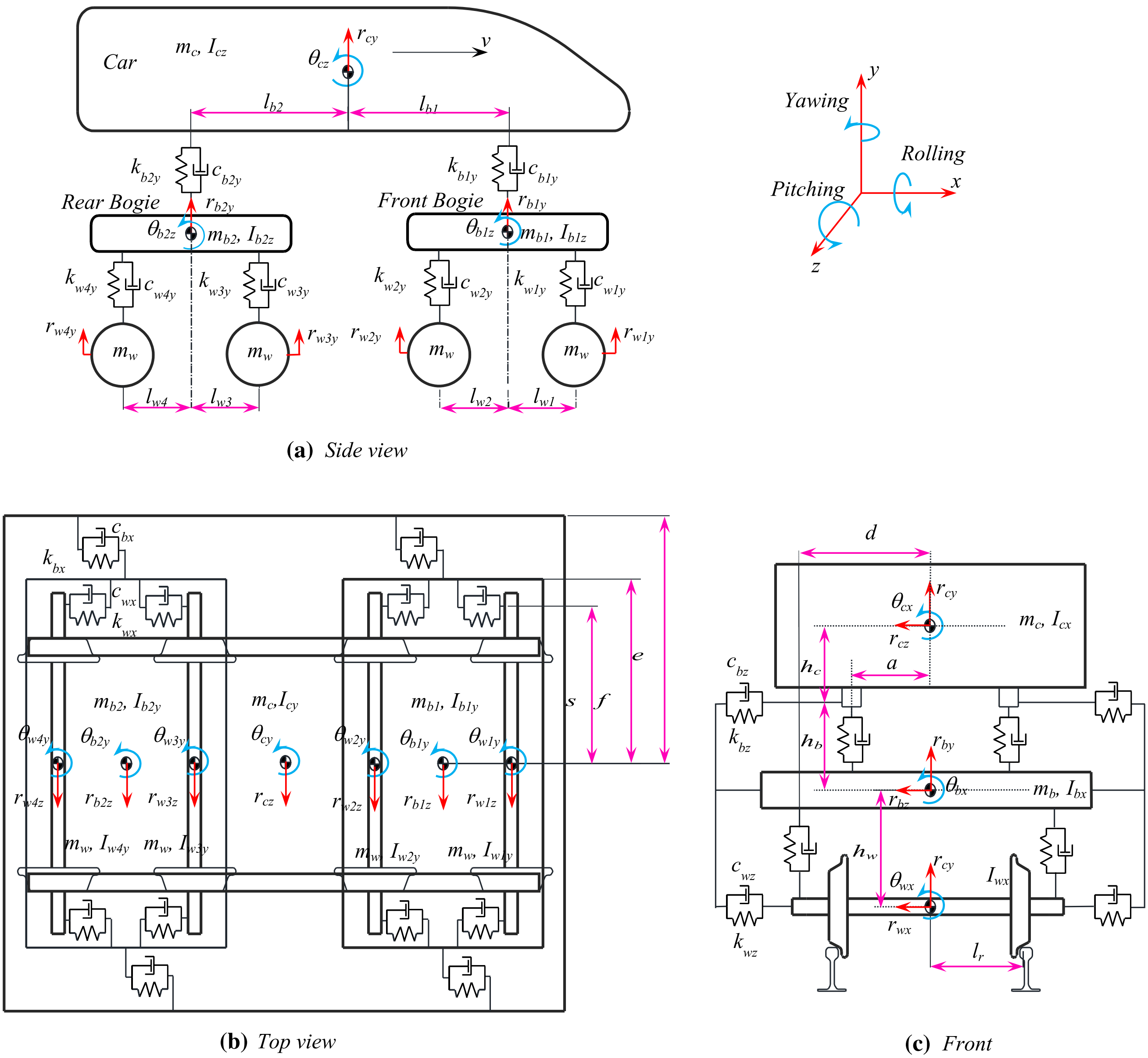

Fig. 2 Railway vehicle mathematical model **a** side view, **b** top view, **c** front view

generalized coordinates of the 3D high-speed train model are shown in Table 2. The introduction of all parameters found in the mathematical model shown in Fig. 2 is in the previous paper [74] by the authors of this article.

Equation of Motion of the Train Model

In this paper, the motion equations of the high-speed train model in Fig. 1 were obtained by using the Lagrange method. The high-speed train model's potential energy, kinetic energy, and Rayleigh dissipation function expressions

Table 1 The full 3D high-speed train's parameters

The mass of train body (m_c)	40 tons	Lateral damping of the secondary suspension system ($c_{biz}, i=1,2$)	10 kNs/m
Bogie masses ($m_{b1}=m_{b2}$)	3.04 tons	The longitudinal damping of the secondary suspension system ($c_{bix}, i=1,2$)	100 kNs/m
Wheels mass ($m_{wi}, i=1,2,3,4$)	1.78 tons	The primary suspension system's vertical damping ($c_{wiy}, i=1,2,3,4$)	90.2 kNs/m
Car's mass moment of inertia around pitch motion (I_{cz})	2080 tons m^2	Lateral damping of primary suspension system ($c_{wiz}, i=1,2,3,4$)	10 kNs/m
Car's mass moment of inertia around roll motion (I_{cx})	75 tons m^2	The primary suspension system's longitudinal damping of ($c_{wix}, i=1,2,3,4$)	10 kNs/m
Car's mass moment of inertia around yaw axis (I_{cy})	224 tons m^2	Length of bridge (L)	50 m
Bogies mass moment of inertia around pitch axis ($I_{biz}, i=1,2$)	3.93 tons m^2	Center of gravity of the car and the bogie's longitudinal distance ($l_{bi}, i=1,2$)	8.75 m
Bogies mass moment of inertia around roll axis ($I_{bix}, i=1,2$)	1.9 tons m^2	Bogie's longitudinal separation from the vertical primary suspension ($l_{wi}, i=1,2,3,4$)	1.25 m
Bogies mass moment of inertia around yaw axis ($I_{biy}, i=1,2$)	2.1 tons m^2	Vertical distance from bogie to lateral primary suspension (h_w)	0.22 m
Wheels mass moment of inertia around roll axis ($I_{wix}, i=1,2,3,4$)	1.25 tons m^2	Vertical distance from car to lateral secondary suspension (h_c)	0.8 m
Wheels mass moment of inertia around yaw axis ($I_{wiy}, i=1,2,3,4$)	1.4 tons m^2	Vertical distance from bogie to lateral secondary suspension (h_b)	0.5 m
Vertical stiffness of secondary suspension system ($k_{biy}, i=1,2$)	1180 kN/m	Half of secondary suspension spacing (a)	1 m
Lateral stiffness of secondary suspension system ($k_{biz}, i=1,2$)	15,000 kN/m	Half of wheelset contact distance (l_r)	0.7175 m
The secondary suspension system's longitudinal stiffness ($k_{bix}, i=1,2$)	10,000 kN/m	Half of primary spacing (d)	1 m
The primary suspension system's vertical stiffness ($k_{wiy}, i=1,2,3,4$)	530 kN/m	Half of bogie spacing (f)	1 m
The primary suspension system's Lateral stiffness ($k_{wiz}, i=1,2,3,4$)	350 kN/m	Side-to-side separation between the wheelset and the longitudinal secondary suspension (s)	0.9 m
The primary suspension system's longitudinal stiffness ($k_{wix}, i=1,2,3,4$)	340 kN/m	Side-to-side separation between the wheelset and the longitudinal primary suspension (e)	1.2 m
The secondary suspension system's Vertical damping ($c_{biy}, i=1,2$)	39.2 kNs/m		

Table 2 Generalized high-speed train model coordinates

Parameter	Vertical motion	Lateral motion	Pitch motion	Roll motion	Yaw motion
Car	r_{cy}	r_{cz}	Θ_{cz}	Θ_{cx}	Θ_{cy}
Front bogie	r_{b1y}	r_{b1z}	Θ_{b1z}	Θ_{b1x}	Θ_{b1y}
Rear bogie	r_{b2y}	r_{b2z}	Θ_{b2z}	Θ_{b2x}	Θ_{b2y}
1st wheelset	r_{w1y}	r_{w1z}		Θ_{w1x}	Θ_{w1y}
2nd wheelset	r_{w2y}	r_{w2z}		Θ_{w2x}	Θ_{w2y}
3rd wheelset	r_{w3y}	r_{w3z}		Θ_{w3x}	Θ_{w3y}
4th wheelset	r_{w4y}	r_{w4z}		Θ_{w4x}	Θ_{w4y}

having the parameters given in Table 1 are expressed in Eqs. (1a–c).

$$E_k=\frac{1}{2}\left[\begin{array}{c}\int_0^L \mu_{R,r}\left[\dot{w}^2_{R,r}(x,t)\right]dx+\int_0^L \mu_{R,b}\left[\dot{w}^2_{R,b}(x,t)\right]dx+\int_0^L \mu_{L,r}\left[\dot{w}^2_{L,r}(x,t)\right]dx+\int_0^L \mu_{L,b}\left[\dot{w}^2_{L,b}(x,t)\right]dx\\ +m_c\dot{r}^2_{cy}+m_c\dot{r}^2_{cz}+I_{cz}\dot{\theta}^2_{cz}+I_{cx}\dot{\theta}^2_{cx}+I_{cy}\dot{\theta}^2_{cy}+m_{b1}\dot{r}^2_{b1y}+m_{b1}\dot{r}^2_{b1z}+I_{b1z}\dot{\theta}^2_{b1z}+I_{b1x}\dot{\theta}^2_{b1x}+I_{b1y}\dot{\theta}^2_{b1y}\\ +m_{b2}\dot{r}^2_{b2y}+m_{b2}\dot{r}^2_{b2z}+I_{b2z}\dot{\theta}^2_{b2z}+I_{b2x}\dot{\theta}^2_{b2x}+I_{b2y}\dot{\theta}^2_{b2y}+m_w\dot{r}^2_{w1y}+m_w\dot{r}^2_{w1z}+I_{w1x}\dot{\theta}^2_{w1x}+I_{w1y}\dot{\theta}^2_{w1y}\\ +m_w\dot{r}^2_{w2y}+m_w\dot{r}^2_{w2z}+I_{w2x}\dot{\theta}^2_{w2x}+I_{w2y}\dot{\theta}^2_{w2y}+m_w\dot{r}^2_{w3y}+m_w\dot{r}^2_{w3z}+I_{w3x}\dot{\theta}^2_{w3x}+I_{w3y}\dot{\theta}^2_{w3y}+m_w\dot{r}^2_{w4y}\\ +m_w\dot{r}^2_{w4z}+I_{w4x}\dot{\theta}^2_{w4x}+I_{w4y}\dot{\theta}^2_{w4y}+m_{R,s}\dot{w}^2_{R,s}+m_{R,ba}\dot{w}^2_{R,ba}+m_{L,s}\dot{w}^2_{L,s}+m_{L,ba}\dot{w}^2_{L,ba}\end{array}\right] \tag{1a}$$

$$E_p=\frac{1}{2}\left[\begin{array}{c}\int_0^L E_{R,r}I_{R,r}\left[{w''}^2_{R,r}(x,t)\right]dx+\int_0^L E_{R,b}I_{R,b}\left[{w''}^2_{R,b}(x,t)\right]dx+\int_0^L E_{L,r}I_{L,r}\left[{w''}^2_{L,r}(x,t)\right]dx+\int_0^L E_{L,b}I_{L,b}\left[{w''}^2_{L,b}(x,t)\right]dx\\ +k_{b1y}\left[r_{cy}-r_{b1y}+\theta_{cz}l_{b1}-\theta_{cx}a+\theta_{b1x}a\right]^2+k_{b1y}\left[r_{cy}-r_{b1y}+\theta_{cz}l_{b1}+\theta_{cx}a-\theta_{b1x}a\right]^2\\ +k_{b2y}\left[r_{cy}-r_{b2y}-\theta_{cz}l_{b2}-\theta_{cx}a+\theta_{b2x}a\right]^2+k_{b2y}\left[r_{cy}-r_{b2y}-\theta_{cz}l_{b2}+\theta_{cx}a-\theta_{b2x}a\right]^2\\ +k_{w1y}\left[r_{b1y}-r_{w1y}+\theta_{b1z}l_{w1}-\theta_{b1x}d+\theta_{w1x}d\right]^2+k_{w1y}\left[r_{b1y}-r_{w1y}+\theta_{b1z}l_{w1}+\theta_{b1x}d-\theta_{w1x}d\right]^2\\ +k_{w2y}\left[r_{b1y}-r_{w2y}-\theta_{b1z}l_{w2}-\theta_{b1x}d+\theta_{w2x}d\right]^2+k_{w2y}\left[r_{b1y}-r_{w2y}-\theta_{b1z}l_{w2}+\theta_{b1x}d-\theta_{w2x}d\right]^2\\ +k_{w3y}\left[r_{b2y}-r_{w3y}+\theta_{b2z}l_{w3}-\theta_{b2x}d+\theta_{w3x}d\right]^2+k_{w3y}\left[r_{b2y}-r_{w3y}+\theta_{b2z}l_{w3}+\theta_{b2x}d-\theta_{w3x}d\right]^2\\ +k_{w4y}\left[r_{b2y}-r_{w4y}-\theta_{b2z}l_{w4}-\theta_{b2x}d+\theta_{w4x}d\right]^2+k_{w4y}\left[r_{b2y}-r_{w4y}-\theta_{b2z}l_{w4}+\theta_{b2x}d-\theta_{w4x}d\right]^2\\ +2k_{bz}\left[r_{cz}-r_{b1z}-\theta_{cx}h_c-\theta_{b1x}h_b\right]^2+2k_{bz}\left[r_{cz}-r_{b2z}-\theta_{cx}h_c-\theta_{b2x}h_b\right]^2+2k_{wz}\left[r_{b1z}-r_{w1z}-\theta_{b1x}h_w\right]^2\\ +2k_{wz}\left[r_{b1z}-r_{w2z}-\theta_{b1x}h_w\right]^2+2k_{wz}\left[r_{b2z}-r_{w3z}-\theta_{b2x}h_w\right]^2+2k_{wz}\left[r_{b2z}-r_{w4z}-\theta_{b2x}h_w\right]^2\\ +2k_{bx}\left[\theta_{cy}e-\theta_{b1y}f\right]^2+2k_{bx}\left[\theta_{cy}e-\theta_{b2y}f\right]^2+2k_{wx}[\theta_{b1y}s-\theta_{w1y}s]^2+2k_{wx}[\theta_{b1y}s-\theta_{w2y}s]^2\\ +2k_{wx}[\theta_{b2y}s-\theta_{w3y}s]^2+2k_{wx}[\theta_{b2y}s-\theta_{w4y}s]^2+k_p\left[w_{r,l}-w_{s,l}\right]^2+k_p\left[w_{r,r}-w_{s,r}\right]^2+k_b\left[w_{s,l}-w_{ba,l}\right]^2\\ +k_b\left[w_{s,r}-w_{ba,r}\right]^2+k_f\left[w_{ba,l}-w_{b,l}\right]^2+k_f\left[w_{ba,r}-w_{b,r}\right]^2\end{array}\right] \tag{1b}$$

$$D=\frac{1}{2}\left[\begin{array}{c}\int_0^L c_{R,r}\dot{w}^2_{R,r}(x,t)dx+\int_0^L c_{R,b}\dot{w}^2_{R,b}(x,t)dx+\int_0^L c_{L,r}\dot{w}^2_{L,r}(x,t)dx+\int_0^L c_{L,b}\dot{w}^2_{L,b}(x,t)dx\\ +c_{b1y}\left[\dot{r}_{cy}-\dot{r}_{b1y}+\dot{\theta}_{cz}l_{b1}-\dot{\theta}_{cx}a+\dot{\theta}_{b1x}a\right]^2+c_{b1y}\left[\dot{r}_{cy}-\dot{r}_{b1y}+\dot{\theta}_{cz}l_{b1}+\dot{\theta}_{cx}a-\dot{\theta}_{b1x}a\right]^2\\ +c_{b2y}\left[\dot{r}_{cy}-\dot{r}_{b2y}-\dot{\theta}_{cz}l_{b2}-\dot{\theta}_{cx}a+\dot{\theta}_{b2x}a\right]^2+c_{b2y}\left[\dot{r}_{cy}-\dot{r}_{b2y}-\dot{\theta}_{cz}l_{b2}+\dot{\theta}_{cx}a-\dot{\theta}_{b2x}a\right]^2\\ +c_{w1y}\left[\dot{r}_{b1y}-\dot{r}_{w1y}+\dot{\theta}_{b1z}l_{w1}-\dot{\theta}_{b1x}d+\dot{\theta}_{w1x}d\right]^2+c_{w1y}\left[\dot{r}_{b1y}-\dot{r}_{w1y}+\dot{\theta}_{b1z}l_{w1}+\dot{\theta}_{b1x}d-\dot{\theta}_{w1x}d\right]^2\\ +c_{w2y}\left[\dot{r}_{b1y}-\dot{r}_{w2y}-\dot{\theta}_{b1z}l_{w2}-\dot{\theta}_{b1x}d+\dot{\theta}_{w2x}d\right]^2+c_{w2y}\left[\dot{r}_{b1y}-\dot{r}_{w2y}-\dot{\theta}_{b1z}l_{w2}+\dot{\theta}_{b1x}d-\dot{\theta}_{w2x}d\right]^2\\ +c_{w3y}\left[\dot{r}_{b2y}-\dot{r}_{w3y}+\dot{\theta}_{b2z}l_{w3}-\dot{\theta}_{b2x}d+\dot{\theta}_{w3x}d\right]^2+c_{w3y}\left[\dot{r}_{b2y}-\dot{r}_{w3y}+\dot{\theta}_{b2z}l_{w3}+\dot{\theta}_{b2x}d-\dot{\theta}_{w3x}d\right]^2\\ +c_{w4y}\left[\dot{r}_{b2y}-\dot{r}_{w4y}-\dot{\theta}_{b2z}l_{w4}-\dot{\theta}_{b2x}d+\dot{\theta}_{w4x}d\right]^2+c_{w4y}\left[\dot{r}_{b2y}-\dot{r}_{w4y}-\dot{\theta}_{b2z}l_{w4}+\dot{\theta}_{b2x}d-\dot{\theta}_{w4x}d\right]^2\\ +2c_{bz}\left[\dot{r}_{cz}-\dot{r}_{b1z}-\dot{\theta}_{cx}h_c-\dot{\theta}_{b1x}h_b\right]^2+2c_{bz}\left[\dot{r}_{cz}-\dot{r}_{b2z}-\dot{\theta}_{cx}h_c-\dot{\theta}_{b2x}h_b\right]^2+2c_{wz}\left[\dot{r}_{b1z}-\dot{r}_{w1z}-\dot{\theta}_{b1x}h_w\right]^2\\ +2c_{wz}\left[\dot{r}_{b1z}-\dot{r}_{w2z}-\dot{\theta}_{b1x}h_w\right]^2+2c_{wz}\left[\dot{r}_{b2z}-\dot{r}_{w3z}-\dot{\theta}_{b2x}h_w\right]^2+2c_{wz}\left[\dot{r}_{b2z}-\dot{r}_{w4z}-\dot{\theta}_{b2x}h_w\right]^2\\ +2c_{bx}\left[\dot{\theta}_{cy}e-\dot{\theta}_{b1y}f\right]^2+2c_{bx}\left[\dot{\theta}_{cy}e-\dot{\theta}_{b2y}f\right]^2+c_{wx}\left[\dot{\theta}_{b1y}s-\dot{\theta}_{w1y}s\right]^2+2c_{wx}\left[\dot{\theta}_{b1y}s-\dot{\theta}_{w2y}s\right]^2\\ +2c_{wx}\left[\dot{\theta}_{b2y}s-\dot{\theta}_{w3y}s\right]^2+2c_{wx}\left[\dot{\theta}_{b2y}s-\dot{\theta}_{w4y}s\right]^2+c_p\left[\dot{w}_{r,l}-\dot{w}_{s,l}\right]^2+c_p\left[\dot{w}_{r,r}-\dot{w}_{s,r}\right]^2\\ +c_b\left[\dot{w}_{s,l}-\dot{w}_{ba,l}\right]^2+c_b\left[\dot{w}_{s,r}-\dot{w}_{ba,r}\right]^2+c_f\left[\dot{w}_{ba,l}-\dot{w}_{b,l}\right]^2+c_f\left[\dot{w}_{ba,r}-\dot{w}_{b,r}\right]^2\end{array}\right] \tag{1c}$$

In Eqs. 1a–1c, $\mu_{R,r}$, $\mu_{L,r}$, $\mu_{R,b}$, and $\mu_{L,b}$ are the right and left rail beam and bridge beam's mass of the unit length, respectively. $E_{Rr}I_{R,r}$, $E_{Lr}I_{L,r}$, $E_{Rb}I_{R,b}$, and $E_{L,b}I_{L,b}$ are the flexural rigidity of the right and left rail beam and bridge beams, respectively. On the other hand, Eq. (1c), considering the physical model shown in Fig. 2, can be used to figure out the dissipation function of the whole railway model and flexible structure coupled system. The symbols $c_{R,r}$, $c_{L,r}$, $c_{R,b}$, and $c_{L,b}$ given in Eq. (1c) represent the right and left equivalent viscous damping coefficients for rail beams and bridge beams. The Lagrange expression equals the difference between the kinetic energy and the potential energy given in Eqs. (1a, b) which can be found as ($L=E_k$-E_p), where η_k are the generalized coordinates of the train.

$$\frac{d}{dt}\left(\frac{\partial L}{\partial \dot{\boldsymbol{\eta}}_k(t)}\right)-\frac{\partial L}{\partial \boldsymbol{\eta}_k(t)}+\frac{\partial D}{\partial \dot{\boldsymbol{\eta}}_k(t)}=0, k=1,2,....,31 \tag{2}$$

The equation of motion of the 31-DOFs full train model seen in Fig. 1 are derived using the Lagrange method in Eq. 2 as follows:

The car body's motion equations:

$$\ddot{r}_{cy}=\frac{1}{m_c}\begin{bmatrix}-2c_{b1y}\left[\dot{r}_{cy}-\dot{r}_{b1y}+\dot{\theta}_{cz}l_{b1}\right]-2c_{b2y}\left[\dot{r}_{cy}-\dot{r}_{b2y}-\dot{\theta}_{cz}l_{b2}\right]\\-2k_{b1y}\left[r_{cy}-r_{b1y}+\theta_{cz}l_{b1}\right]-2k_{b2y}\left[r_{cy}-r_{b2y}-\theta_{cz}l_{b2}\right]\end{bmatrix} \tag{3a}$$

$$\ddot{r}_{cz}=\frac{1}{m_c}\left[-2c_{bz}\left[2\dot{r}_{cz}-\dot{r}_{b1z}-\dot{r}_{b2z}-2\dot{\theta}_{cx}h_c-\dot{\theta}_{b1x}h_b-\dot{\theta}_{b2x}h_b\right]-2k_{bz}\left[2r_{cz}-r_{b1z}-r_{b2z}-2\theta_{cx}h_c-\theta_{b1x}h_b-\theta_{b2x}h_b\right]\right] \tag{3b}$$

$$\ddot{\theta}_{cz}=\frac{1}{I_{cz}}\begin{bmatrix}-2c_{b1y}l_{b1}\left[\dot{r}_{cy}-\dot{r}_{b1y}+\dot{\theta}_{cz}l_{b1}\right]+2c_{b2y}l_{b2}\left[\dot{r}_{cy}-\dot{r}_{b2y}-\dot{\theta}_{cz}l_{b2}\right]\\-2k_{b1y}l_{b1}\left[r_{cy}-r_{b1y}+\theta_{cz}l_{b1}\right]+2k_{b2y}l_{b2}\left[r_{cy}-r_{b2y}-\theta_{cz}l_{b2}\right]\end{bmatrix} \tag{3c}$$

$$\ddot{\theta}_{cx}=\frac{1}{I_{cx}}\left[-2c_{b1y}a^2\left[\dot{\theta}_{cx}-\dot{\theta}_{b1x}\right]-2c_{b2y}a^2\left[\dot{\theta}_{cx}-\dot{\theta}_{b2x}\right]-2k_{b1y}a^2\left[\theta_{cx}-\theta_{b1x}\right]-2k_{b2y}a^2\left[\theta_{cx}-\theta_{b2x}\right]\right] \tag{3d}$$

$$\ddot{\theta}_{cy}=\frac{1}{I_{cy}}\left[-2c_{bx}e\left[2\dot{\theta}_{cy}e-\dot{\theta}_{b1y}f-\dot{\theta}_{b2y}f\right]-2k_{bx}e\left[2\theta_{cy}e-\theta_{b1y}f-\theta_{b2y}f\right]\right] \tag{3e}$$

The motion equations of front bogie have been written as Eqs. (3f, j):

$$\ddot{r}_{b1y}=\frac{1}{m_{b1}}\begin{bmatrix}2c_{b1y}\left[\dot{r}_{cy}-\dot{r}_{b1y}+\dot{\theta}_{cz}l_{b1}\right]-c_{w1y}\left[2\dot{r}_{b1y}-\varphi_i(\xi_{1R},t)\dot{q}_i-\varphi_i(\xi_{1L},t)\dot{q}_i+2\dot{\theta}_{b1z}l_{w1}\right]\\-c_{w2y}\left[2\dot{r}_{b1y}-\varphi_i(\xi_{2R},t)\dot{q}_i-\varphi_i(\xi_{2L},t)\dot{q}_i-2\dot{\theta}_{b1z}l_{w2}\right]+2k_{b1y}\left[r_{cy}-r_{b1y}+\theta_{cz}l_{b1}\right]\\-k_{w1y}\left[2r_{b1y}-\varphi_i\left(\xi_{1R},t\right)q_i-\varphi_i\left(\xi_{1L},t\right)q_i+2\theta_{b1z}l_{w1}\right]\\-k_{w2y}\left[2r_{b1y}-\varphi_i(\xi_{2R},t)q_i-\varphi_i(\xi_{2L},t)q_i-2\theta_{b1z}l_{w2}\right]\end{bmatrix} \tag{3f}$$

$$\ddot{r}_{b1z}=\frac{1}{m_{b1}}\begin{bmatrix}2c_{bz}\left[\dot{r}_{cz}-\dot{r}_{b1z}-\dot{\theta}_{cx}h_c+\dot{\theta}_{b1x}h_b\right]-2c_{wz}\left[2\dot{r}_{b1z}-\dot{r}_{w1z}-\dot{r}_{w2z}-2\dot{\theta}_{b1x}h_w\right]\\+2k_{bz}\left[r_{cz}-r_{b1z}-\theta_{cx}h_c+\theta_{b1x}h_b\right]-2k_{wz}\left[2r_{b1z}-r_{w1z}-r_{w2z}-2\theta_{b1x}h_w\right]\end{bmatrix} \tag{3g}$$

$$\ddot{\theta}_{b1z}=\frac{1}{I_{b1z}}\begin{bmatrix}c_{w2y}l_{w2}\left[2\dot{r}_{b1y}-\varphi_i\left(\xi_{2R},t\right)\dot{q}_i-\varphi_i\left(\xi_{2L},t\right)\dot{q}_i-2\dot{\theta}_{b1z}l_{w2}\right]\\-c_{w1y}l_{w1}\left[2\dot{r}_{b1y}-\varphi_i(\xi_{1R},t)\dot{q}_i-\varphi_i(\xi_{1L},t)\dot{q}_i+2\dot{\theta}_{b1z}l_{w1}\right]\\-k_{w1y}l_{w1}\left[2r_{b1y}-\varphi_i\left(\xi_{1R},t\right)q_i-\varphi_i\left(\xi_{1L},t\right)q_i+2\theta_{b1z}l_{w1}\right]\\+k_{w2y}l_{w2}\left[2r_{b1y}-\varphi_i(\xi_{2R},t)q_i-\varphi_i(\xi_{2L},t)q_i-2\theta_{b1z}l_{w2}\right]\end{bmatrix} \tag{3h}$$

$$\ddot{\theta}_{b1x}=\frac{1}{I_{b1x}}\begin{bmatrix} 2c_{b1y}a^2\left[\dot{\theta}_{cx}-\dot{\theta}_{b1x}\right]+c_{w1y}d\left[2\dot{\theta}_{w1x}d-\varphi_i(\xi_{1R},t)\dot{q}_i+\varphi_i(\xi_{1L},t)\dot{q}_i-2\dot{\theta}_{b1x}d\right] \\ +c_{w2y}d\left[2\dot{\theta}_{w2x}d-\varphi_i(\xi_{2R},t)\dot{q}_i+\varphi_i(\xi_{2L},t)\dot{q}_i-2\dot{\theta}_{b1x}d\right]+2k_{b1y}a^2\left[\theta_{cx}-\theta_{b1x}\right] \\ +k_{w1y}d\left[2\theta_{w1x}d-\varphi_i(\xi_{1R},t)q_i+\varphi_i(\xi_{1L},t)q_i-2\theta_{b1x}d\right] \\ +k_{w2y}d\left[2\theta_{w2x}d-\varphi_i(\xi_{2R},t)q_i+\varphi_i(\xi_{2L},t)q_i-2\theta_{b1x}d\right] \end{bmatrix} \tag{3i}$$

$$\ddot{\theta}_{b1y}=\frac{1}{I_{b1y}}\begin{bmatrix} 2c_{bx}f\left[\dot{\theta}_{cy}e-\dot{\theta}_{b1y}f\right]-2c_{wx}s^2\left[2\dot{\theta}_{b1y}-\dot{\theta}_{w1y}-\dot{\theta}_{w2y}\right] \\ +2k_{bx}f\left[\theta_{cy}e-\theta_{b1y}f\right]-2k_{wx}s^2\left[2\theta_{b1y}-\theta_{w1y}-\theta_{w2y}\right] \end{bmatrix} \tag{3j}$$

The following are the rear bogie's motion equations:

$$\ddot{r}_{b2y}=\frac{1}{m_{b2}}\begin{bmatrix} 2c_{b2y}\left[\dot{r}_{cy}-\dot{r}_{b2y}-\dot{\theta}_{cz}l_{b2}\right]-c_{w3y}\left[2\dot{r}_{b2y}-\varphi_i(\xi_{3R},t)\dot{q}_i-\varphi_i(\xi_{3L},t)\dot{q}_i+2\dot{\theta}_{b2z}l_{w3}\right] \\ -c_{w4y}\left[2\dot{r}_{b2y}-\varphi_i(\xi_{4R},t)\dot{q}_i-\varphi_i(\xi_{4L},t)\dot{q}_i-2\dot{\theta}_{b2z}l_{w4}\right]+2k_{b2y}\left[r_{cy}-r_{b2y}-\theta_{cz}l_{b2}\right] \\ -k_{w3y}\left[2r_{b2y}-\varphi_i(\xi_{3R},t)q_i-\varphi_i(\xi_{3L},t)q_i+2\theta_{b2z}l_{w3}\right] \\ -k_{w4y}\left[2r_{b2y}-\varphi_i(\xi_{4R},t)q_i-\varphi_i(\xi_{4L},t)q_i-2\theta_{b2z}l_{w4}\right] \end{bmatrix} \tag{3k}$$

$$\ddot{r}_{b2z}=\frac{1}{m_{b2}}\begin{bmatrix} 2c_{bz}\left[\dot{r}_{cz}-\dot{r}_{b2z}-\dot{\theta}_{cx}h_c-\dot{\theta}_{b2x}h_b\right]-2c_{wz}\left[2\dot{r}_{b2z}-\dot{r}_{w3z}-\dot{r}_{w4z}-2\dot{\theta}_{b2x}h_w\right] \\ +2k_{bz}\left[r_{cz}-r_{b2z}-\theta_{cx}h_c-\theta_{b2x}h_b\right]-2k_{wz}\left[2r_{b2z}-r_{w3z}-r_{w4z}-2\theta_{b2x}h_w\right] \end{bmatrix} \tag{3l}$$

$$\ddot{\theta}_{b2z}=\frac{1}{I_{b2z}}\begin{bmatrix} c_{w4y}l_{w4}\left[2\dot{r}_{b2y}-\varphi_i(\xi_{4R},t)\dot{q}_i-\varphi_i(\xi_{4L},t)\dot{q}_i-2\dot{\theta}_{b2z}l_{w4}\right] \\ -c_{w3y}l_{w3}\left[2\dot{r}_{b2y}-\varphi_i(\xi_{3R},t)\dot{q}_i-\varphi_i(\xi_{3L},t)\dot{q}_i+2\dot{\theta}_{b2z}l_{w3}\right] \\ k_{w4y}l_{w4}\left[2r_{b2y}-\varphi_i(\xi_{4R},t)q_i-\varphi_i(\xi_{4L},t)q_i-2\theta_{b2z}l_{w4}\right] \\ -k_{w3y}l_{w3}\left[2r_{b2y}-\varphi_i(\xi_{3R},t)q_i-\varphi_i(\xi_{3L},t)q_i+2\theta_{b2z}l_{w3}\right] \end{bmatrix} \tag{3m}$$

$$\ddot{\theta}_{b2x}=\frac{1}{I_{b2x}}\begin{bmatrix} 2c_{b2y}a^2\left[\dot{\theta}_{cx}-\dot{\theta}_{b2x}\right]+c_{w3y}d\left[2\dot{\theta}_{w3x}d-\varphi_i(\xi_{3R},t)\dot{q}_i+\varphi_i(\xi_{3L},t)\dot{q}_i-2\dot{\theta}_{b2x}d\right] \\ +c_{w4y}d\left[2\dot{\theta}_{w4x}d-\varphi_i(\xi_{4R},t)\dot{q}_i+\varphi_i(\xi_{4L},t)\dot{q}_i-2\dot{\theta}_{b2x}d\right]+2k_{b2y}a^2\left[\theta_{cx}-\theta_{b2x}\right] \\ +k_{w3y}d\left[2\theta_{w3x}d-\varphi_i(\xi_{3R},t)q_i+\varphi_i(\xi_{3L},t)q_i-2\theta_{b2x}d\right] \\ +k_{w4y}d\left[2\theta_{w4x}d-\varphi_i(\xi_{4R},t)q_i+\varphi_i(\xi_{4L},t)q_i-2\theta_{b2x}d\right] \end{bmatrix} \tag{3n}$$

$$\ddot{\theta}_{b2y}=\frac{1}{I_{b2y}}\begin{bmatrix} 2c_{bx}f\left[\dot{\theta}_{cy}e-\dot{\theta}_{b2y}f\right]-2c_{wx}s^2\left[2\dot{\theta}_{b2y}-\dot{\theta}_{w3y}-\dot{\theta}_{w4y}\right] \\ +2k_{bx}f\left[\theta_{cy}e-\theta_{b2y}f\right]-2k_{wx}s^2\left[2\theta_{b2y}-\theta_{w3y}-\theta_{w4y}\right] \end{bmatrix} \tag{3o}$$

The wheelsets' equations of motion are provided by Eq. (3p–s). (For $k=1,2$ $j=1$ and for $k=3,4$ $j=2$).

Vertical motion:

$$\ddot{r}_{wky}=\frac{1}{m_w}\left[2c_{wky}\left[\dot{r}_{bjy}-\dot{r}_{wky}+\dot{\theta}_{bjz}l_{wk}\right]+2k_{wky}\left[r_{bjy}-r_{wky}+\theta_{bjz}l_{wk}\right]\right] \tag{3p}$$

Lateral motion:

Fig. 3 The illustration of the track-bridge couple model

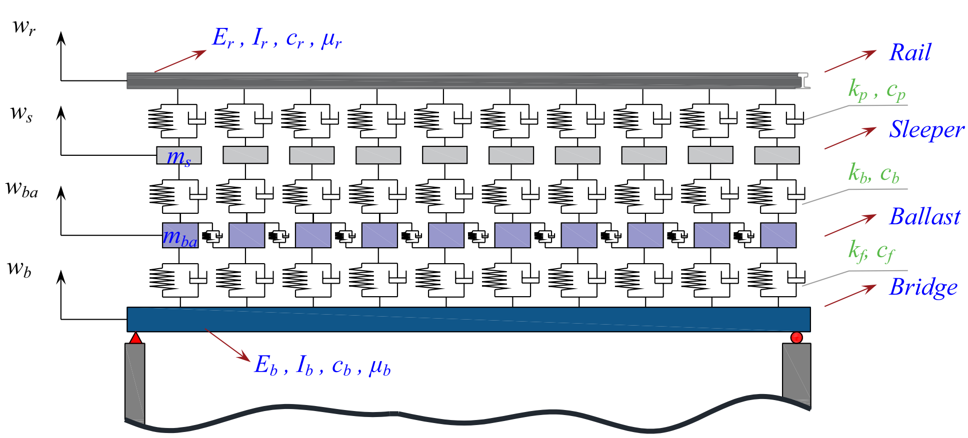

Table 3 The parameters of the track and beams

	Beam parameter			Track parameter			
	Rail	Right bridge	Left bridge				
Modulus of elasticity (GPa)	210	207	200	Sleeper mass (kg)	237	Ballast mass (kg)	683
Cross section inertia moment (m^4)	0.174	0.2	0.2	The stiffness coefficient between the rail and the sleeper (N/m)	1.2×10^8	The damping coefficient between the rail and the sleeper (Ns/m)	1.24×10^5
Mass of unit length (kg/m)	52.5	20,000	18,000	The stiffness coefficient between the sleeper and the ballast (N/m)	2.4×10^8	The damping coefficient between the sleeper and the ballast (Ns/m)	5.88×10^4
Equivalent damping coefficient (Ns/m)	1750	1750	1750	The stiffness coefficient between the ballast and the bridge (N/m)	6.5×10^7	The damping coefficient between the ballast and the bridge (Ns/m)	3.12×10^4

$$\ddot{r}_{wkz} = \frac{1}{m_w}\left[2c_{wz}\left[\dot{r}_{bjz} - \dot{r}_{wkz} - \dot{\theta}_{bjx}h_w\right] + 2k_{wz}\left[r_{bjz} - r_{wkz} - \theta_{bjx}h_w\right]\right] \tag{3q}$$

Roll motion:

$$\ddot{\theta}_{wkx} = \frac{1}{I_{wkx}}\left[\begin{array}{l} c_{wky}d\left[2\dot{\theta}_{bjx}d - \varphi_i(\xi_{kL},t)\dot{q}_i + \varphi_i(\xi_{kR},t)\dot{q}_i - 2\dot{\theta}_{wkx}d\right] \\ +k_{wky}d\left[2\theta_{bjx}d - \varphi_i(\xi_{kL},t)q_i + \varphi_i(\xi_{kR},t)q_i - 2\theta_{wkx}d\right] \end{array}\right] \tag{3r}$$

Yaw motion:

$$\ddot{\theta}_{wky} = \frac{1}{I_{wky}}\left[2c_{wx}s^2\left[\dot{\theta}_{bjy} - \dot{\theta}_{wky}\right] + 2k_{wx}s^2\left[\theta_{bjy} - \theta_{wky}\right]\right] \tag{3s}$$

Motion Equations of the Track-Bridge Subsystem

The track transmits loads from the railway to the bridge or the mainland while simultaneously guiding the train. As shown in Fig. 3, the system specified as track consists of subsystems such as rail, sleeper, ballast, and their connection elements. Between the rail-sleeper, sleeper-ballast, and ballast-bridge, there is only a vertical connection with spring and damping elements with coefficients k_p, k_b, k_f, c_p, c_b, c_f, respectively. While many railways have ballasted tracks, some can be built as ballastless tracks where the tracks are laid on the concrete ground [31]. Different models can be used to perform TTBIS analysis. There is a single-layer model [49, 53, 75–77] in which the rails without ballast and sleepers are placed only on the bridge beam or the mainland, two-layer model [70, 78–80] with only the sleeper with the rail, and multi-layer [71, 81] track models with rail, sleeper, and ballast. The ballast and sub-layers beneath the sleepers are often regarded as distributed equivalent mass components associated with one another in multi-layer track models [31, 73].

Since the track subsystem is more complex, rails are usually modelled using the infinite Euler–Bernoulli or Timoshenko beam theory resting on Winkler elastic foundations. In contrast, the sleeper and ballast are modelled as individual rigid bodies, and the equations of motion are determined [73, 82]. The rail and bridge beam differential equations are given in Eqs. 4 and 5, respectively, using the Euler–Bernoulli beam theorem. Here, E_r and I_r represent the elasticity modulus and the area moment of inertia of the rail beam. w_r represents the vertical displacement of the rail beam at a given time t, μ_r represents the mass of the rail beam's unit length, F represents the total wheel force acting on the rail beam, δ represents the Dirac-Delta function, ω_r represents the circular damping frequency of the rail beam (Table 3). In the other equation, w_b is the vertical displacement of the bridge beam, μ_b stands for the mass per unit length of the bridge beam, ω_b is the circular damping frequency of the bridge beam, E_b and I_b represent the elasticity modulus and area moment of inertia of the bridge beam, respectively. x_r and x_b depict the direction and magnitude of the force, respectively, compared to the left reference of the beam, and its value is found as in Eq. 6.

$$E_rI_r\frac{\partial^4 w_r(x,t)}{\partial x^4} + \mu_r\frac{\partial^2 w_r(x,t)}{\partial t^2} + 2\mu_r\omega_r\frac{\partial w_r(x,t)}{\partial t} = -\sum_{r=1}^{n}F_r\delta\left(x - x_r\right) \tag{4}$$

$$\begin{aligned} &E_bI_b\frac{\partial^4 w_b(x,t)}{\partial x^4} + \mu_b\frac{\partial^2 w_b(x,t)}{\partial t^2} + 2\mu_b\omega_b\frac{\partial w_b(x,t)}{\partial t} \\ &= -\sum_{b=1}^{n}\left[k_f\left(w_{ba} - w_b\right) + c_f\left(\dot{w}_{ba} - \dot{w}_b\right)\right]\delta\left(x - x_b\right) \end{aligned} \tag{5}$$

$$x_1 = vt, x_2 = vt - 2l_w, x_3 = vt - l_{b1} - l_{b2}, x_4 = vt - l_{b1} - l_{b2} - 2l_w, \tag{6}$$

For analytical solution the following serial functions $w_{R,r}(x,t)$, $w_{L,r}(x,t)$, $w_{R,b}(x,t)$, and $w_{L,b}(x,t)$ are considered in the Galerkin's method for the right rail, left rail, right and left bridge beam deflections respectively:

$$\begin{aligned} w_{R,r}(x,t) &= \sum_{i=1}^{n}\varphi_i(x)q_i(t),\ w_{L,r}(x,t) \\ &= \sum_{i=1}^{n}\varphi_{i+n}(x)q_{i+n}(t)w_{R,b}(x,t) \\ &= \sum_{i=1}^{n}\varphi_i(x)\phi_i(t),\ w_{L,b}(x,t) \\ &= \sum_{i=1}^{n}\varphi_{i+n}(x)\phi_{i+n}(t) \end{aligned} \tag{7a}$$

$$\begin{aligned} \dot{w}_{R,r}(x,t) &= \sum_{i=1}^{n}\varphi_i(x)\dot{q}_i(t),\ \dot{w}_{L,r}(x,t) \\ &= \sum_{i=1}^{n}\varphi_{i+n}(x)\dot{q}_{i+n}(t)\,\dot{w}_{R,b}(x,t) \\ &= \sum_{i=1}^{n}\varphi_i(x)\dot{\phi}_i(t),\ \dot{w}_{L,b}(x,t) \\ &= \sum_{i=1}^{n}\varphi_{i+n}(x)\dot{\phi}_{i+n}(t) \end{aligned} \tag{7b}$$

$$\begin{aligned} w''_{R,r}(x,t) &= \sum_{i=1}^{n}\varphi''_i(x)q_i(t),\ w''_{L,r}(x,t) \\ &= \sum_{i=1}^{n}\varphi''_{i+n}(x)q_{i+n}(t)w''_{R,b}(x,t) \\ &= \sum_{i=1}^{n}\varphi''_i(x)\phi_i(t),\ w''_{L,b}(x,t) \\ &= \sum_{i=1}^{n}\varphi''_{i+n}(x)\phi_{i+n}(t) \end{aligned} \tag{7c}$$

Here the symbols ϕ and q are the generalized coordinates for the bridge and rail beams displacements, respectively.

And φ_i is the mode shape of ith mode of the bridge and rail beams and n stands for the maximum mode number considered for the solution. For the simply supported boundary conditions the assumed mode shape functions are:

$$\varphi_i(x) = \sqrt{\frac{2}{L}}sin\left(\frac{i\pi x}{L}\right),\ i = 1,2,\ldots,n \tag{8}$$

The orthogonality conditions are described by:

$$\int_0^L \mu\varphi_i(x)\varphi_j(x)dx = N_i\delta_{ij},\ \int_0^L EI\varphi''_i(x)\varphi''_j(x)dx = \Pi_i\delta_{ij} \tag{9}$$

δ_{ij} is the Kronecker delta. The Lagrange equation for the track system only is derived as:

$$\frac{d}{dt}\left(\frac{\partial L}{\partial\dot{\lambda}_i(t)}\right) - \frac{\partial L}{\partial\lambda_i(t)} + \frac{\partial D}{\partial\dot{\lambda}_i(t)} = Q_i, i = 1,2,....,32 \tag{10}$$

$$Q_i = \int_0^L \varphi_i(x)f_{ci}(x,t)dx,\ i = 1,2,....,32 \tag{11}$$

The generalized coordinates λ_i of the track system are presented in Eq. (12) for the assumed four mode approximated solution.

$$\lambda(t) = \begin{Bmatrix} q_1(t)q_2(t)q_3(t)q_4(t)q_5(t)q_6(t)q_7(t)q_8(t) \\ \gamma_1(t)\gamma_2(t)\gamma_3(t)\gamma_4(t)\gamma_5(t)\gamma_6(t)\gamma_7(t)\gamma_8(t) \\ \psi_1(t)\psi_2(t)\psi_3(t)\psi_4(t)\psi_5(t)\psi_6(t)\psi_7(t)\psi_8(t) \\ \phi_1(t)\phi_2(t)\phi_3(t)\phi_4(t)\phi_5(t)\phi_6(t)\phi_7(t)\phi_8(t) \end{Bmatrix}^T, \left\langle \begin{matrix} q \to \text{Rail beam} \\ \gamma \to \text{Sleeper} \\ \psi \to \text{Ballast} \\ \phi \to \text{Bridge beam} \end{matrix} \right\rangle \tag{12}$$

The orthogonality conditions provided in Eq. 9 and the Galerkin's approach described in Eqs. 7a–7c were used to generate the equation of motion for the track subsystem shown in Fig. 3. In Eqs. (13a–13d), the motion equations for the track parts and bridge beam are all given.

For the rail beam:

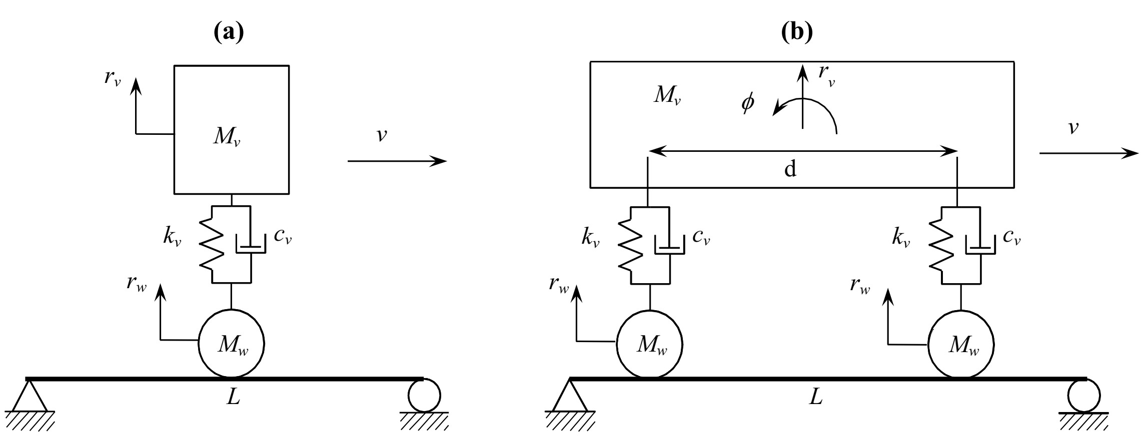

Fig. 4 Validation models **a** one-axle vehicle: moving sprung mass model; **b** two-axle vehicle: suspended rigid beam model

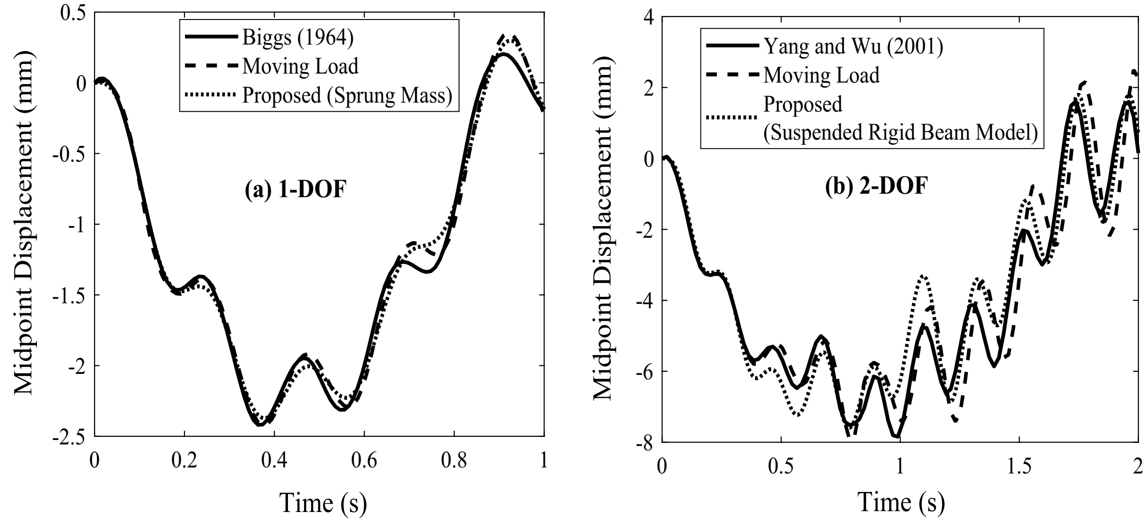

Fig. 5 Comparing both models with proposed method **a** case 1: one-axle vehicle, **b** two-axle vehicle

$$
\begin{aligned}
&\ddot{q}_{i(t)} = -S_1 q_{i(t)}/N_1 - c_1 \dot{q}_{i(t)}/N_1 + \varphi_i(\xi_{1R},t)/N_1 \\
&\Big[c_{w1y}\Big[\dot{r}_{b1y} - \textstyle\sum_{i=1}^{n}\varphi_i(\xi_{1R},t)\dot{q}_i + \dot{\theta}_{b1z}l_{w1} - \dot{\theta}_{b1x}d + \dot{\theta}_{w1x}d\Big] \\
&+k_{w1y}\Big[r_{b1y} - \textstyle\sum_{i=1}^{n}\varphi_i(\xi_{1R},t)q_i + \theta_{b1z}l_{w1} - \theta_{b1x}d + \theta_{w1x}d\Big] - fg_1\Big] \\
&+\varphi_i(\xi_{2R},t)/N_1\Big[c_{w2y}\Big[\dot{r}_{b1y} - \textstyle\sum_{i=1}^{n}\varphi_i(\xi_{2R},t)\dot{q}_i - \dot{\theta}_{b1z}l_{w2} - \dot{\theta}_{b1x}d + \dot{\theta}_{w2x}d\Big] \\
&+k_{w2y}\Big[r_{b1y} - \textstyle\sum_{i=1}^{n}\varphi_i(\xi_{2R},t)q_i - \theta_{b1z}l_{w2} - \theta_{b1x}d + \theta_{w2x}d\Big] - fg_2\Big] \\
&+\varphi_i(\xi_{3R},t)/N_1\Big[c_{w3y}\Big[\dot{r}_{b2y} - \textstyle\sum_{i=1}^{n}\varphi_i(\xi_{3R},t)\dot{q}_i + \dot{\theta}_{b2z}l_{w3} - \dot{\theta}_{b2x}d + \dot{\theta}_{w3x}d\Big] \\
&+k_{w3y}\Big[r_{b2y} - \textstyle\sum_{i=1}^{n}\varphi_i(\xi_{3R},t)q_i + \theta_{b2z}l_{w3} - \theta_{b2x}d + \theta_{w3x}d\Big] - fg_3\Big] \\
&+\varphi_i(\xi_{4R},t)/N_1\Big[c_{w4y}\Big[\dot{r}_{b2y} - \textstyle\sum_{i=1}^{n}\varphi_i(\xi_{4R},t)\dot{q}_i - \dot{\theta}_{b2z}l_{w4} - \dot{\theta}_{b2x}d + \dot{\theta}_{w4x}d\Big] \\
&+k_{w4y}\Big[r_{b2y} - \textstyle\sum_{i=1}^{n}\varphi_i(\xi_{4R},t)q_i - \theta_{b2z}l_{w4} - \theta_{b2x}d + \theta_{w4x}d\Big] - fg_4\Big]
\end{aligned}
\tag{13a}
$$

For the sleeper:

$$
\begin{aligned}
\ddot{w}_{s,r} = \frac{1}{m_s}\Big[&k_p\big[w_{r,r} - w_{s,r}\big] - k_b\big[w_{s,r} - w_{ba,r}\big] \\
&+c_p\big[\dot{w}_{r,r} - \dot{w}_{s,r}\big] - c_b\big[\dot{w}_{s,r} - \dot{w}_{ba,r}\big]\Big]
\end{aligned}
\tag{13b}
$$

For the ballast:

$$
\begin{aligned}
\ddot{w}_{ba,r} = \frac{1}{m_{ba}}\Big[&k_b\big[w_{s,r} - w_{ba,r}\big] \\
&-k_f\big[w_{ba,r} - w_{b,r}\big] + c_b\big[\dot{w}_{s,r} - \dot{w}_{ba,r}\big] \\
&-c_f\big[\dot{w}_{ba,r} - \dot{w}_{b,r}\big]\Big]
\end{aligned}
\tag{13c}
$$

For the bridge beam:

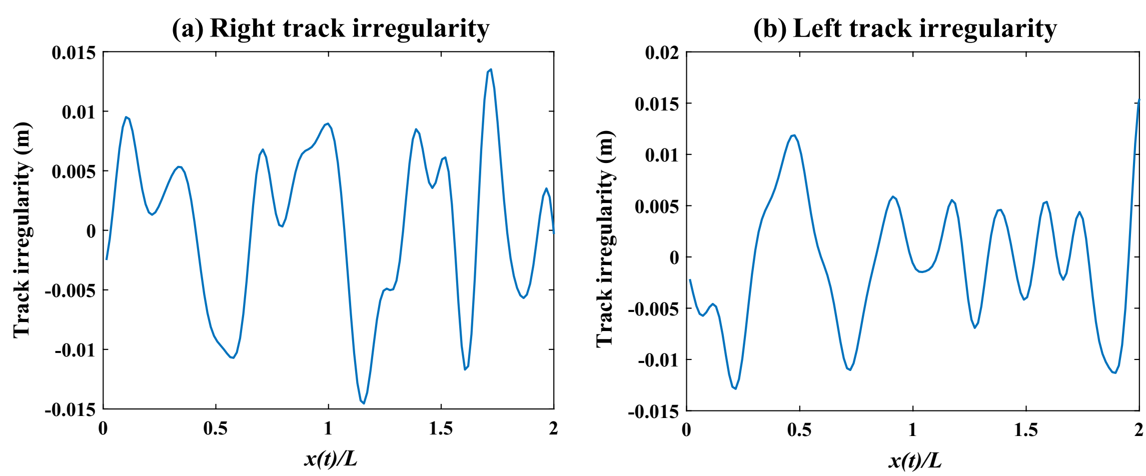

Fig. 6 Random irregularity acting on the right and left track

$$\begin{aligned}\ddot{\phi}_{i(t)} &= -Sb_1\phi_{i(t)}/N_{b1} - cb_1\dot{\phi}_{i(t)}/N_{b1} \\ &- c_f\varphi_i(\xi_R, t)/N_{b1}\left[\dot{w}_{ba,R} - \sum_{i=1}^{n}\varphi_i(\xi_R, t)\dot{\phi}_i\right] \\ &- k_f\varphi_i(\xi_R, t)/N_{b1}\left[w_{ba,R} - \sum_{i=1}^{n}\varphi_i(\xi_R, t)\phi_i\right]\end{aligned} \tag{13d}$$

Numerical Solution

Considering the motions of train car body system, track system and the bridge beam totally sixty-three second order differential equation are derived then they transformed the state-space form. A fourth order Runge–Kutta method given in Appendix A is adopted for the solution of resulting equations.

Validation

The 3D train, track and bridge model examined in this study is a complex system since it has many degrees of freedom. In order to verify this complex system solution, a simpler system has been preferred in the literature. In this section, the one-axle moving vehicle model given in Fig. 4a is considered to validate the present method with the literature [9, 27, 53, 68, 83]. The beam's elasticity module is $E = 2.87$ GPa, its inertia moment is $I = 2.9$ m^4, its mass per unit length is $\mu = 2303$ kg/m, its length is $L = 25$ m, the sprung mass is $M_v = 5750$ kg, the mass of wheel is $M_w = 0$, the spring stiffness is $k_v = 1595 \times 10^3$ N/m, and its damping is zero ($c_v = 0$).

The beam elasticity module was assumed to be $E = 2.943$ GPa in the other validation case, which was connected to the wheel's body through spring and damping elements. The inertia moment of the cross-sectional area was assumed to be $I = 8.65$ m^4, the mass of the beam per unit length was assumed to be $\mu = 36$ tons/m, the beam length was assumed to be $L = 30$ m, and the sprung mass was assumed to be $M_v = 540$ tons. It was estimated that the train would travel at a speed of 27.78 m/s and that there would be $d = 17.5$ m between each pair of wheels.

Figure 5 displays the comparison between the strategy employed in this paper and the examples in Fig. 4. The first verification example examined was previously conducted by Biggs [27], while the second was performed by Yang and Wu [68]. Both the validation instances and the research technique produced outcomes that were quite comparable.

Random Track Irregularity

Train vibrations are the main cause of bridge vibrations, and track irregularities are considered secondary sources. The following is how the inverse Fourier transform can be used to create and study track irregularities in the random category [69].

$$r(x) = \sum_{k=1}^{N} \sqrt{4A_r\left(\omega_k/\omega_o\right)^{-2}\Delta\omega}\cos(\omega_k x - \varphi_k) \tag{14}$$

Here, the irregularity profile is denoted by $r(x)$, and A_r is a size parameter. The discontinuity frequency and waves number are represented, respectively, by the expressions $\omega_k = k\Delta\omega$ and $\omega_o = 1/2\pi$. $\Delta\omega$, frequency increment, x denotes the train's distance from the bridge, and φ_k denotes a randomly generated number between 0 and 2π. N represents the total number of terms used to assess the surface roughness of the rail. Given in Fig. 6 are the independent left and right track irregularities derived from these data. As shown in the equation below, the obtained track profile is combined with the $w_b(x,t)$ formula, which describes the vertical rail motion in the TTBIS system's energy equations. Here, the equations for the beam's velocity, displacement, and acceleration are provided.

$$y = w_b(x, t) + r(x) \tag{15}$$

$$\frac{dy}{dt} = \frac{\partial w_b}{\partial x}\frac{dx}{dt} + \frac{\partial w_b}{\partial t} + \frac{dr}{dx}\frac{dx}{dt} \tag{16}$$

$$\begin{aligned}\frac{d^2y}{dt^2} &= \frac{\partial^2 w_b}{\partial x^2}\left(\frac{dx}{dt}\right)^2 + 2\frac{\partial^2 w_b}{\partial x\partial t}\frac{dx}{dt} + \frac{\partial^2 r}{\partial x^2}\left(\frac{dx}{dt}\right)^2 \\ &+ \frac{\partial w_b}{\partial x}\frac{d^2x}{dt^2} + \frac{\partial^2 w_b}{\partial t^2} + \frac{dr}{dx}\frac{d^2x}{dt^2}\end{aligned} \tag{17}$$

Numerical Analysis of Full 3D High-Speed TTBIS Dynamics

In this study, simulations of the dynamic behaviour of high-speed TTBIS were conducted to ensure the train's driving safety and passenger comfort in different states of the train, track, and bridge. The commercial analytical tool MATLAB was used to analyze the dynamic responses during the high-speed train passage across the track-bridge subsystem, which may be described as the Euler–Bernoulli beam. Table 1 lists the characteristics of the train, track, and bridge beam for study. A comparison was made between the analysis' findings and those of the research reported in the literature in order to confirm its accuracy. Each parameter was chosen at the same for both solutions compared. The Newmark β method was used to analyze the equation of motion for the train models in the literature [64, 77, 84, 85]. The Runge–Kutta method was used to analyze the second-order differential equations in this study after being decreased to a first-order equation in the state space form.

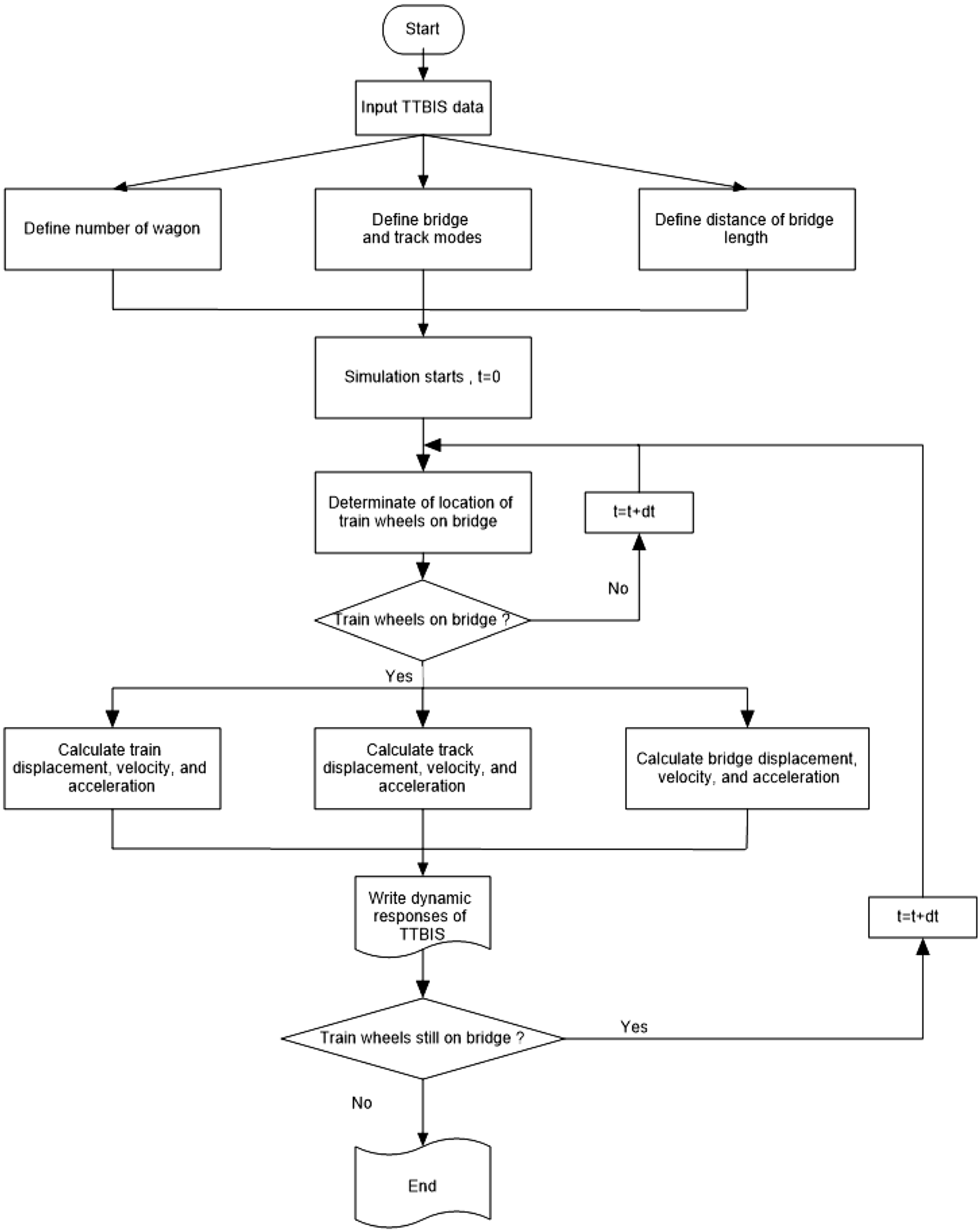

Fig. 7 Flow chart of the proposed TTBIS simulation program

The Flow-Chart Algorithm for the TTBIS

For the proposed train-track-bridge interaction model, a software called TTBIS has been developed, which offers extensive usage possibilities. This software includes only 31-DOFs full train models, a track model consisting of rail, sleeper, and ballast, and a simply supported beam model that can be modelled according to the Euler–Bernoulli beam theorem. In other words, the entire system consists of five separate subsystems: train, track, bridge, train-track couple, and track-bridge couple.

TTBIS software simulation offers a wide range of options to its user. In order to achieve this, first of all, the equations of motion of each the train-track-bridge systems must be obtained and solved. Since first order differential equations will be used in the solving method used in this software simulation system, the equations of motion obtained are used in the software by reducing them. Then, a time step is decided in order to realize a precise and fast solution. If this time step is too small, the analysis resolution time increases considerably, while if it is too coarse, the dynamic responses obtained are not realistic.

In the software program, using the state-space form, the motion equations are reduced to first-order differential equations. The displacement and velocity responses for each degree of freedom are calculated using the time-integration method in a tiny time step. The acceleration values of each degree of freedom can be determined by the variable velocity responses at minimal time intervals.

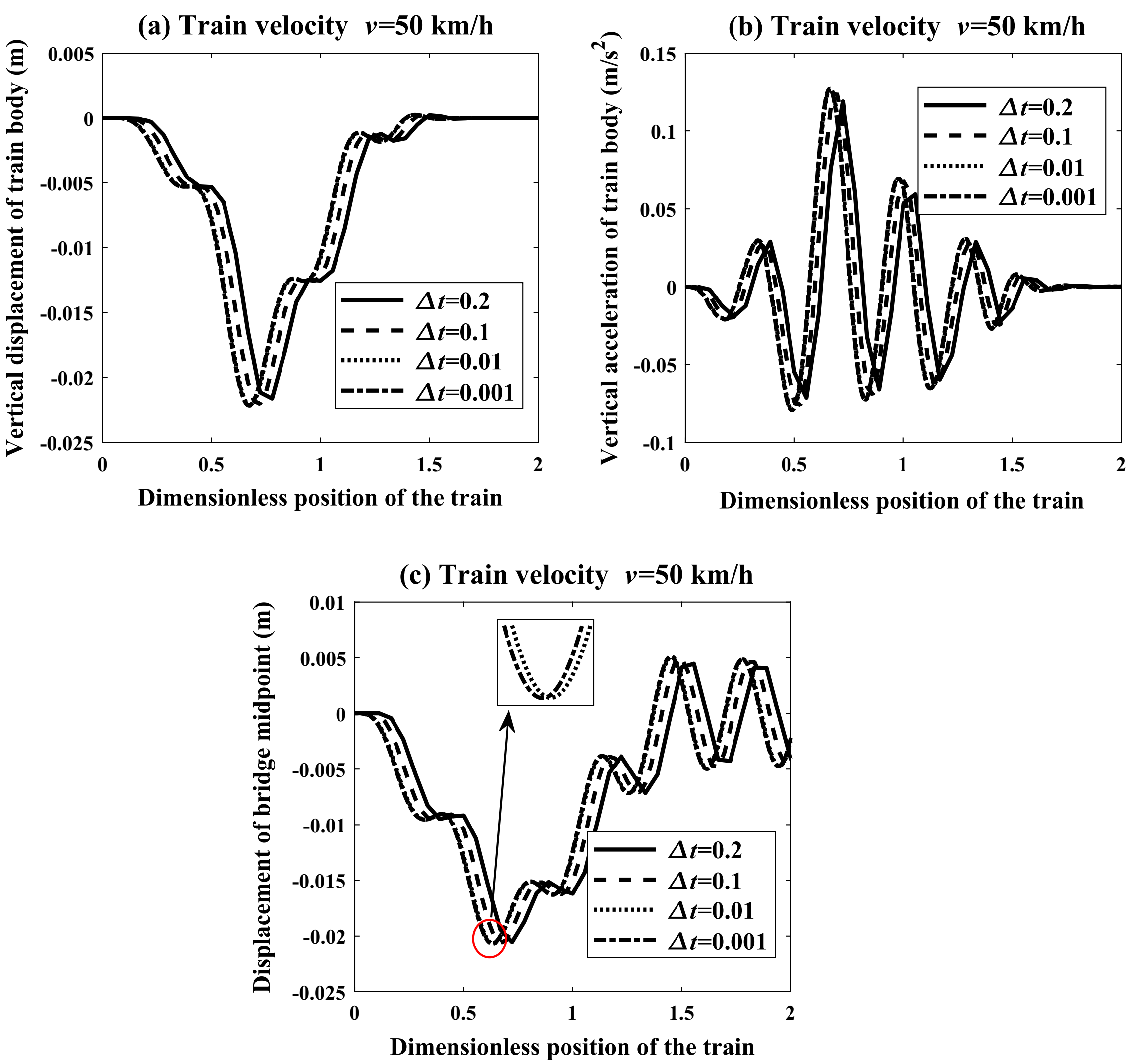

Fig. 8 Time step size Δt effect on the dynamic responses when the train is moving at a speed of 50 km/h: **a** vertical displacement of the train body, **b** vertical acceleration of the train body, **c** displacement of the bridge's midpoint

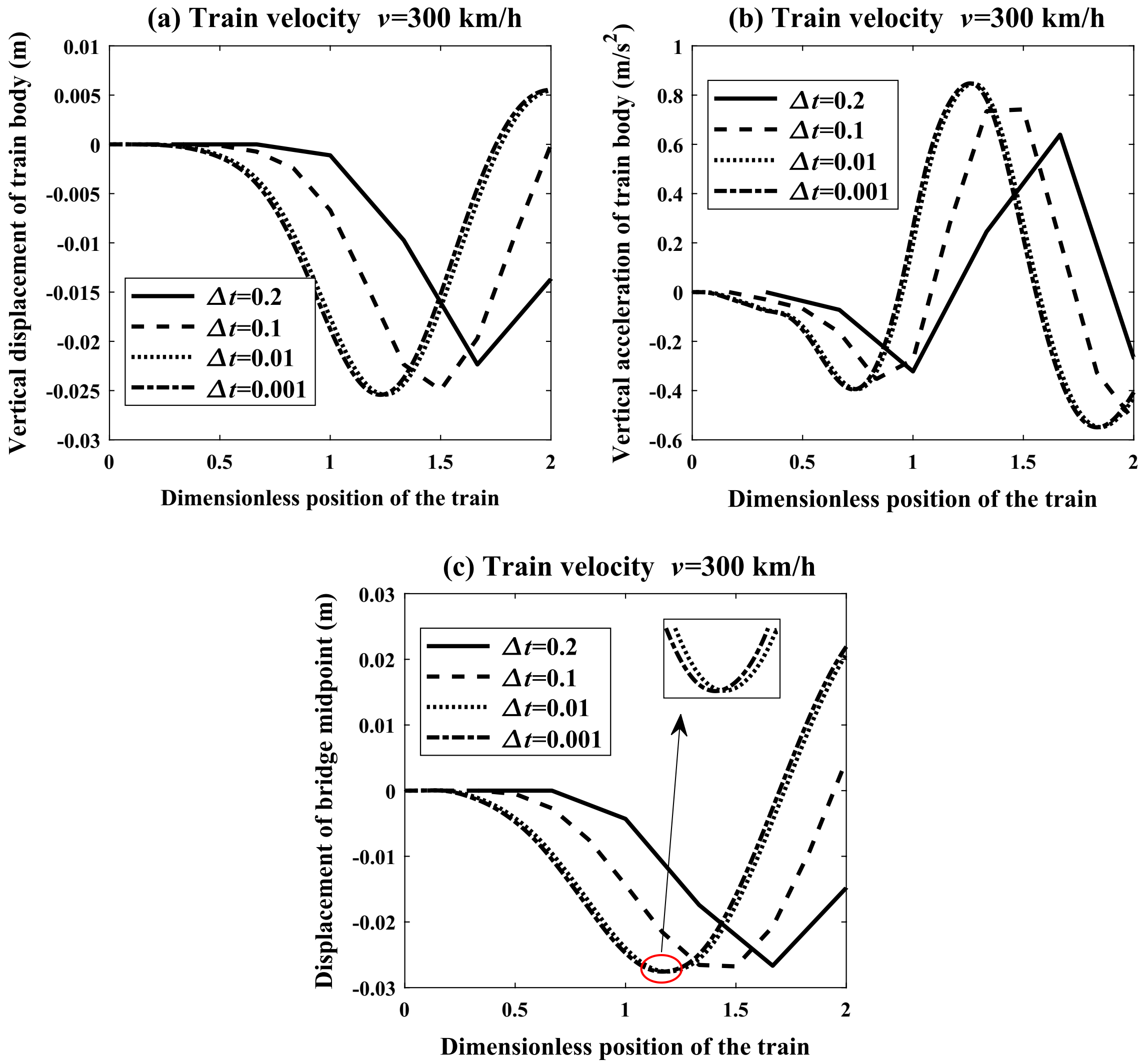

Fig. 9 Time step size effect (Δt) on the dynamic responses when the train is moving at a speed of 300 km/h: **a** vertical displacement of the train body, **b** vertical acceleration of the train body, **c** displacement of the bridge's midpoint

Table 4 Time step size Δt effect on bridge midpoint displacement solution accuracy

Δt (s)	Solution time (s)		RMS (m)		Relative difference (%)		Rate of increase for time (%)	
	50kmh^{-1}	300kmh^{-1}	50kmh^{-1}	300kmh^{-1}	50kmh^{-1}	300kmh^{-1}	50kmh^{-1}	300kmh^{-1}
Bridge midpoint displacement								
0.2	12.70	3.55	0.009362	0.01399	0.7106	17.657	–	–
0.1	12.74	4.22	0.009372	0.01605	0.5409	5.5327	0.31	18.87
0.01	19.61	4.81	0.009423	0.01693	0.0636	0.3531	54.41	35.49
0.001	156.18	28.50	0.009429	0.01699	–	–	1129.76	702.82
Train body displacement								
0.2	12.70	3.55	0.007913	0.010629	0.8023	12.698	–	–
0.1	12.74	4.22	0.007931	0.011665	0.5767	4.1971	0.31	18.87
0.01	19.61	4.81	0.007973	0.012130	0.0576	0.3696	54.41	35.49
0.001	156.18	28.50	0.007977	0.012175	–	–	1129.76	702.82

In Fig. 7, the flow chart of the TTBIS software program is given.

Thanks to this software simulation developed, vertical, lateral, and rotational movements of all parts of the train and all vertical movements of the track and bridge can be determined. In this software, the train's velocity, the characteristics and the length of the bridge that the train passes through, the rail and bridge modelled as a beam, and the vibration mode number of the track can be determined at desired values. In addition, in this TTBIS software, more than one wagon, each of which is a full train model of 31-DOFs, and more than one number of bridges, can be modelled as a Euler–Bernoulli beam can be examined.

The Impact of Time Step on the Dynamic Responses

The Runge–Kutta method is used in this paper to solve the motion equations precisely and accurately for the TTBIS provided in Eqs. (3a–s) and Eqs. (13a–d). The choice of the time step is a key idea in this context. In several studies, it has been recommended to solve the TTBIS's motion equations using various time increments (Figs. 8, 9). For instance, due to low-frequency vibration in the bridge subsystem, Zhu et al. chose a coarse time-step, whereas high-frequency wheel-rail contact in the train and track subsystems required a fine time step [71].

Froio et al. used an automated computation approach to assess the time step for each simulation in their work on determining maximum beam displacements [86]. In order to get the numerical solution of the initial-value issue, they also employed the HHT-implementation approach [87].

This paper calculated the solution step time as Δt before the analysis began. It is sufficient to include $\Delta t = 10^{-2}$ s in the analysis. The findings obtained are unchanged when the solution step time is reduced, but the analysis time is longer. The required time is $(l_{b1} + l_{b2} + l_{w1} + l_{w4})/v = 0.24$ s

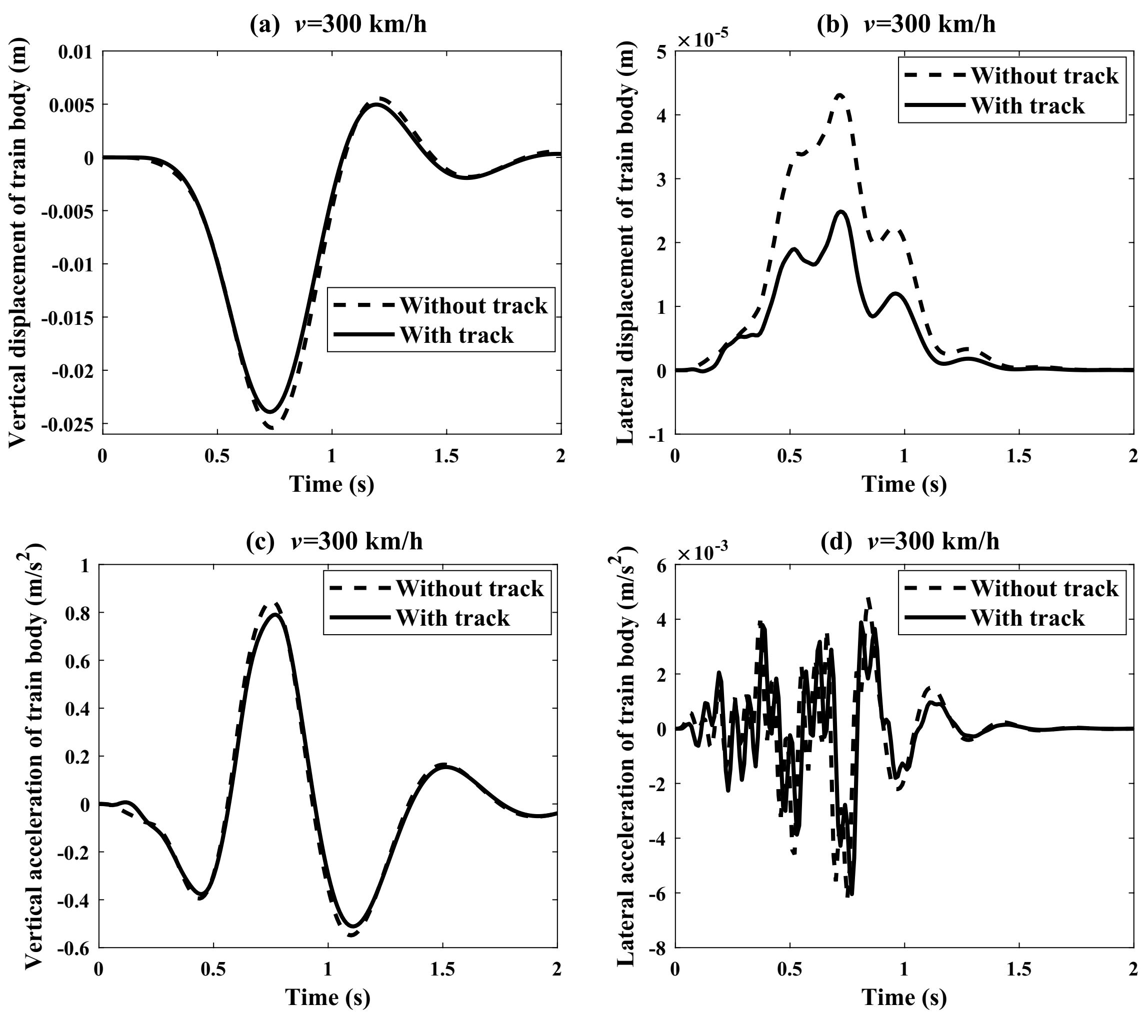

Fig. 10 Time histories of the train body's displacement and acceleration **a** vertical displacement of train body, **b** lateral displacement of train body, **c** vertical acceleration of train body, **d** Lateral acceleration of train body

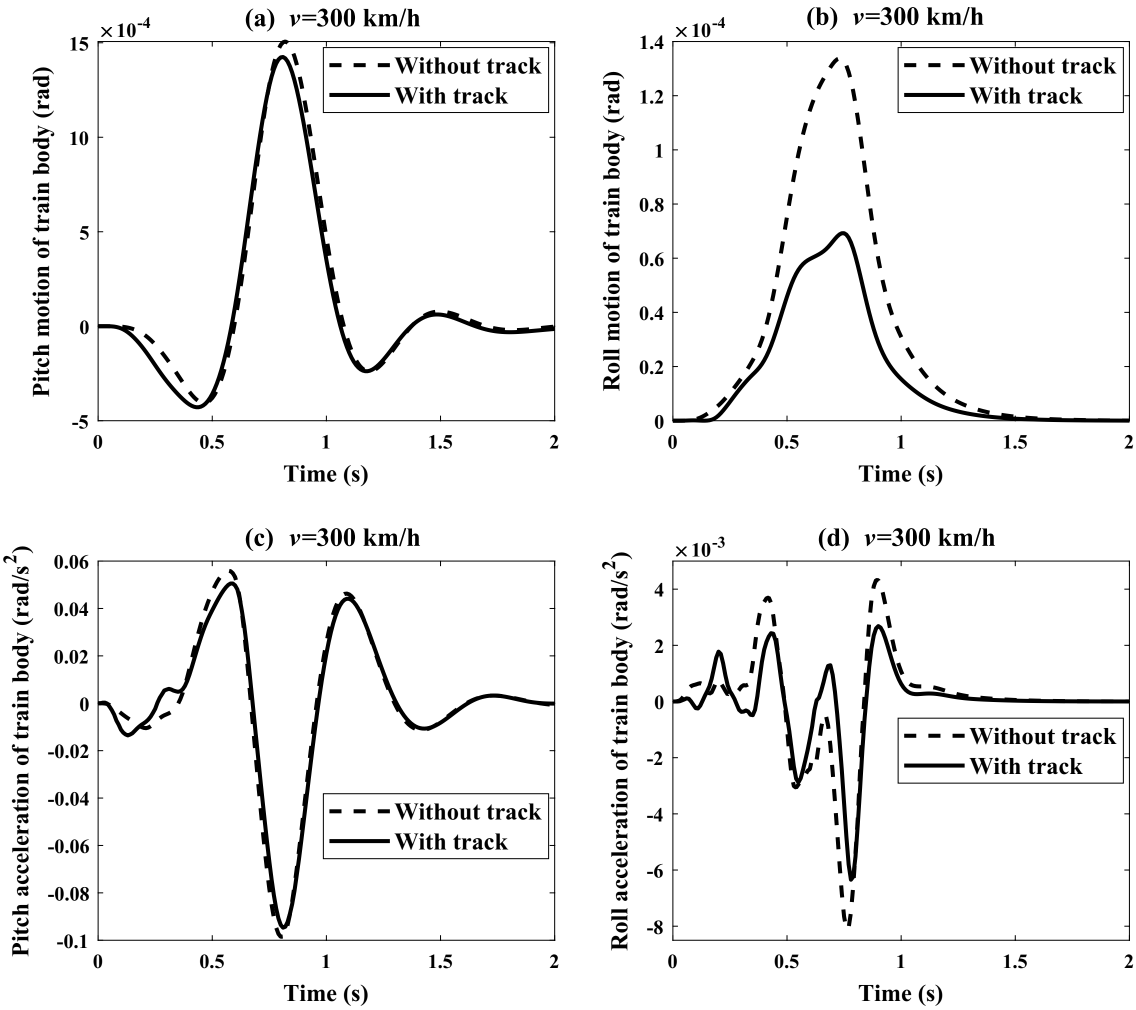

Fig. 11 Time histories of the train body's rotation and angular acceleration **a** pitch motion of train body, **b** roll motion of train body, **c** pitch acceleration of train body, **d** roll acceleration of train body

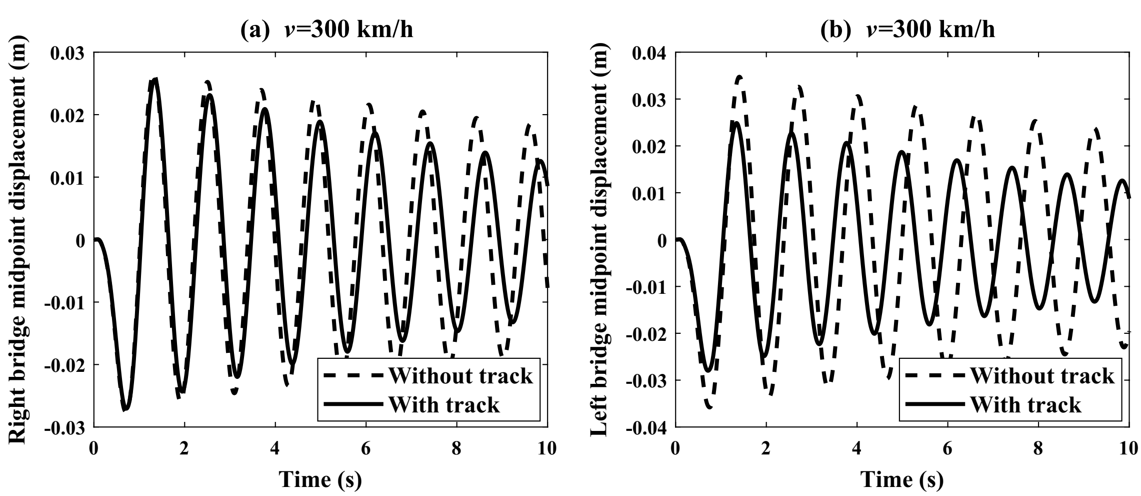

Fig. 12 Time histories of the bridge midpoint displacement **a** midpoint displacement of right bridge, **b** midpoint displacement of left bridge

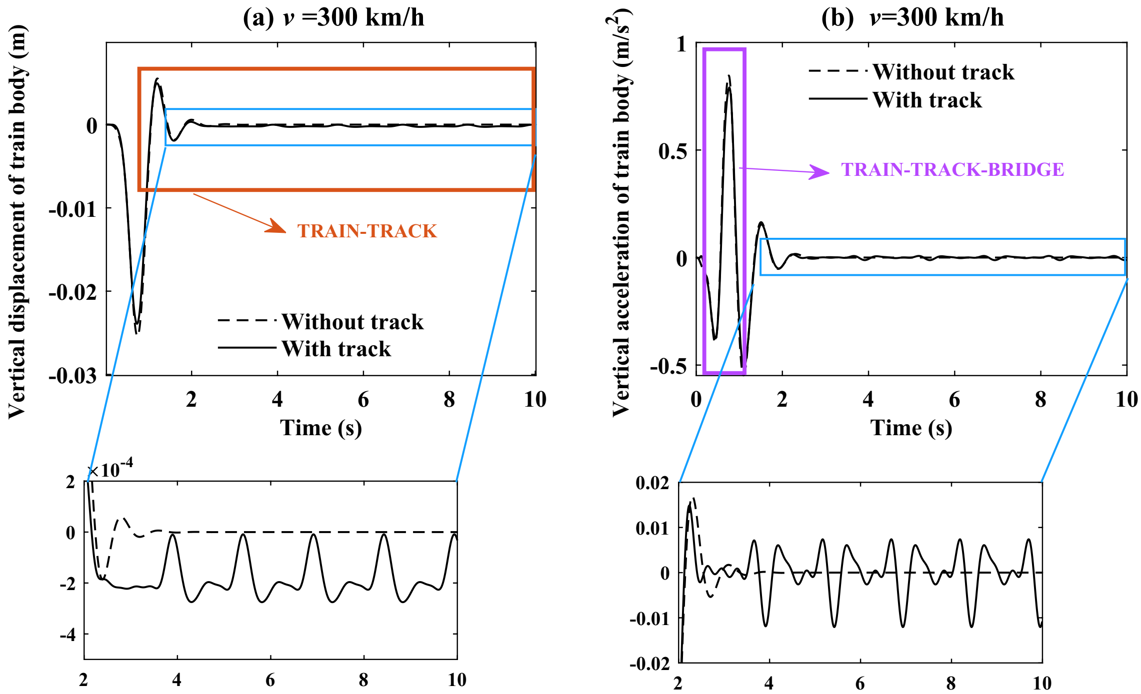

Fig. 13 The track foundation effect upon vehicle dynamic **a** train body's vertical displacement, **b** train body's vertical acceleration

for all wheelsets to make contact with the bridge (Table 4). The train must completely cross the bridge in $(L+l_{b1}+l_{b2}+l_{w1}+l_{w4})/v=0.84$ s. The whole train's departure from the bridge was given a total analysis time of 10 s, and the bridge's dynamic reaction was then examined.

Responses of Train Dynamic for Constant Train Velocity *v* = 300 km/h

In this study, a 3D high-speed train moving on a flexible beam with a discretely supported continuous rail track for numerical simulation, as seen in Fig. 1, was investigated. The bridge and train parameters used by [30, 88] in the literature for simulation in this paper are given in Table 1. In this section, only one vehicle with constant velocity, *v*, passes over the flexible foundation. Also, bridge length and other track and train parameters are given in Table 1. Before starting the TTBIS simulation analysis, the mode function of the rail and bridge modelled as beams was decided. This paper considers the first four modes of track and bridge beam. Additionally, the TBI model without track in the analysis and the TTBIS models with track were compared.

In Figs. 10, 11, the dynamic responses of the train body, depending on whether the railway line is with track (TTBIS) or without track (TBI), are compared if the train speed is 300 km/h bridge length is 50 m. Figure 10a shows that the maximum vertical train body displacement is 0.025 m for TBI and 0.024 m for TTBIS. Similarly, according to the

Table 5 First four vibration mode frequency of the beams and critical velocities of TTBIS.

Mod number	1	2	3	4
Right bridge				
f (*Hz*)	0.91	3.62	8.14	14.46
v_{cr} (m/s)	18.08	72.32	162.72	289.28
Left bridge				
f (*Hz*)	0.94	3.75	8.43	14.99
v_{cr} (m/s)	18.73	74.93	168.59	299.72

vertical train body acceleration in Fig. 10c, it is seen that it is 0.84 m/s^2 for TBI, while it is 0.79 m/s^2 for TTBIS. It is understood that the track structure improves the vertical train dynamic responses by 4% to 6%. Whereas the maximum lateral train body displacement in Fig. 10b is 4.31×10^{-5} m in the TBI model, this is almost halved in the TTBIS model. However, it is shown that the maximum lateral acceleration values of the train body are remarkably like each other, according to Fig. 10d.

In Fig. 11, the train body's pitch and roll motions due to the displacement of the bridge and track while passing over the bridge are given. When Fig. 11 is examined, the train's pitch motion is quite like the vertical motion of the train mentioned in Fig. 10. In Fig. 11a, c, the train's maximum pitch motion is determined to be slightly less in the TTBIS model compared to the TBI model, while in Fig. 11b, d, the largest roll motion for the TTBIS model is quite different from the TBI model. In Fig. 12, the displacement of both bridge beams is given comparatively according to both models. Figure 12a, b show that the bridge displacements are slightly decreased in the TTBIS model. However, in Fig. 12b, it was determined that this decrease was higher than the other. It is understood that the effect of dynamic responses of bridge beams with distinctive characteristics can be eliminated thanks to the track structure.

In Fig. 13, the train body acceleration and displacement are given according to the train velocity being constant at 300 km/h. As mentioned before, the time needed for the train to completely cross the bridge was calculated to be 0.84 s. In this case, the TTBIS is examined at this period, while the train-track interaction system is examined in the part after this period. When the simulation without track is examined in Fig. 13, it is seen that while the vertical dynamic responses of the train are damped after the train leaves the bridge, minimal oscillations continue in the simulation analysis with the track. It is understood that the track subsystem consists of a flexible structure like the bridge subsystem and affects the train's dynamic responses even in the absence of a bridge.

Effect of Bridge Length and Train Velocity

For bridge engineering, bridge parameters are crucial. As shown in Fig. 1, the bridge length that the high-speed train crosses cannot be regarded as constant, and varied bridge lengths alter the dynamic interaction between the train, track, and bridge. The bridge is made to vibrate when the train enters it at a specified speed. The bridge oscillations are quite strong if this velocity is equal to the resonance frequency of the bridge. Moving the train at travel speeds corresponding to the resonance frequency can derail the train or collapse the bridge. Therefore, the train should not be traveling at critical speeds of the bridge. Generally, the train speed should be at least 25% higher than the critical

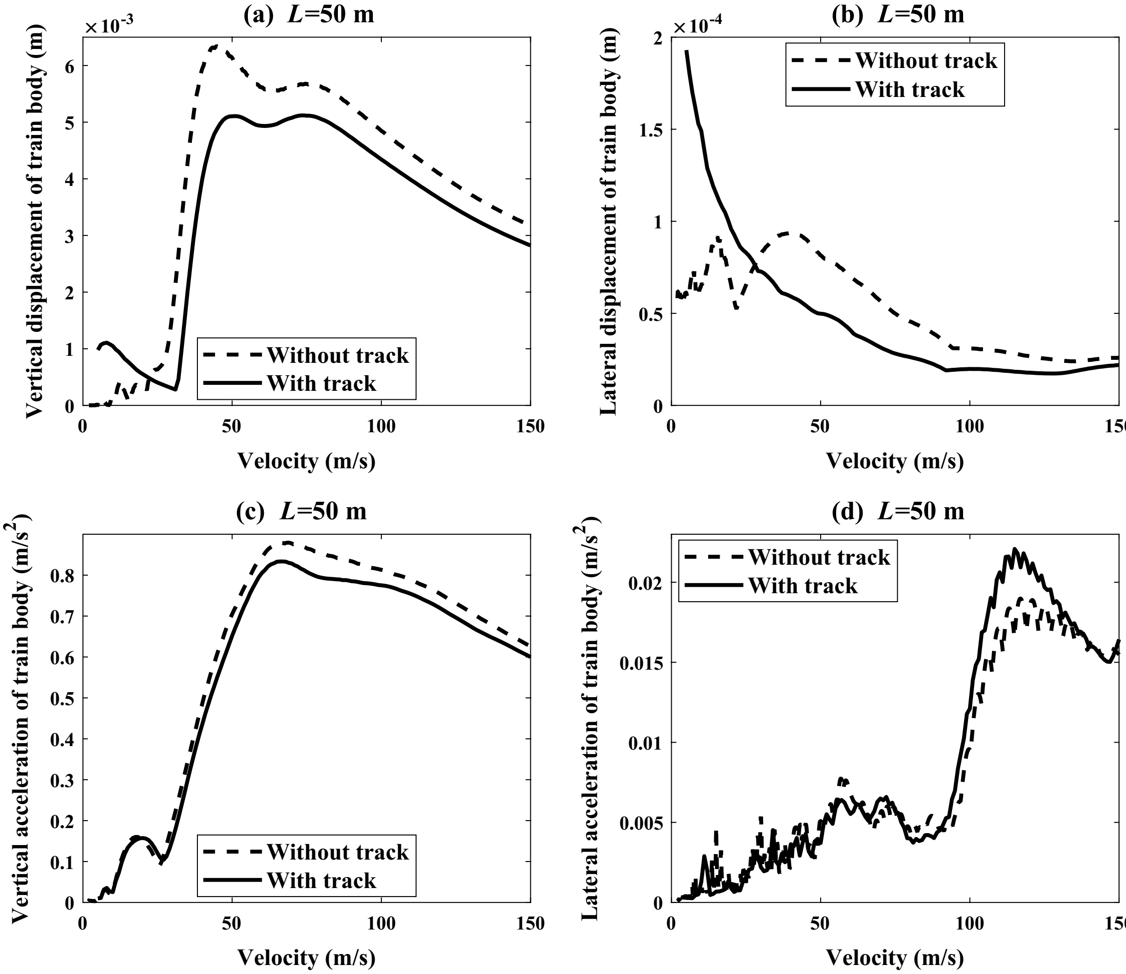

Fig. 14 Comparison of the with track and without track model results of the train body dynamic responses versus train velocity **a** vertical displacement of train body, **b** lateral displacement of train body, **c** vertical acceleration of train body, **d** lateral acceleration of train body

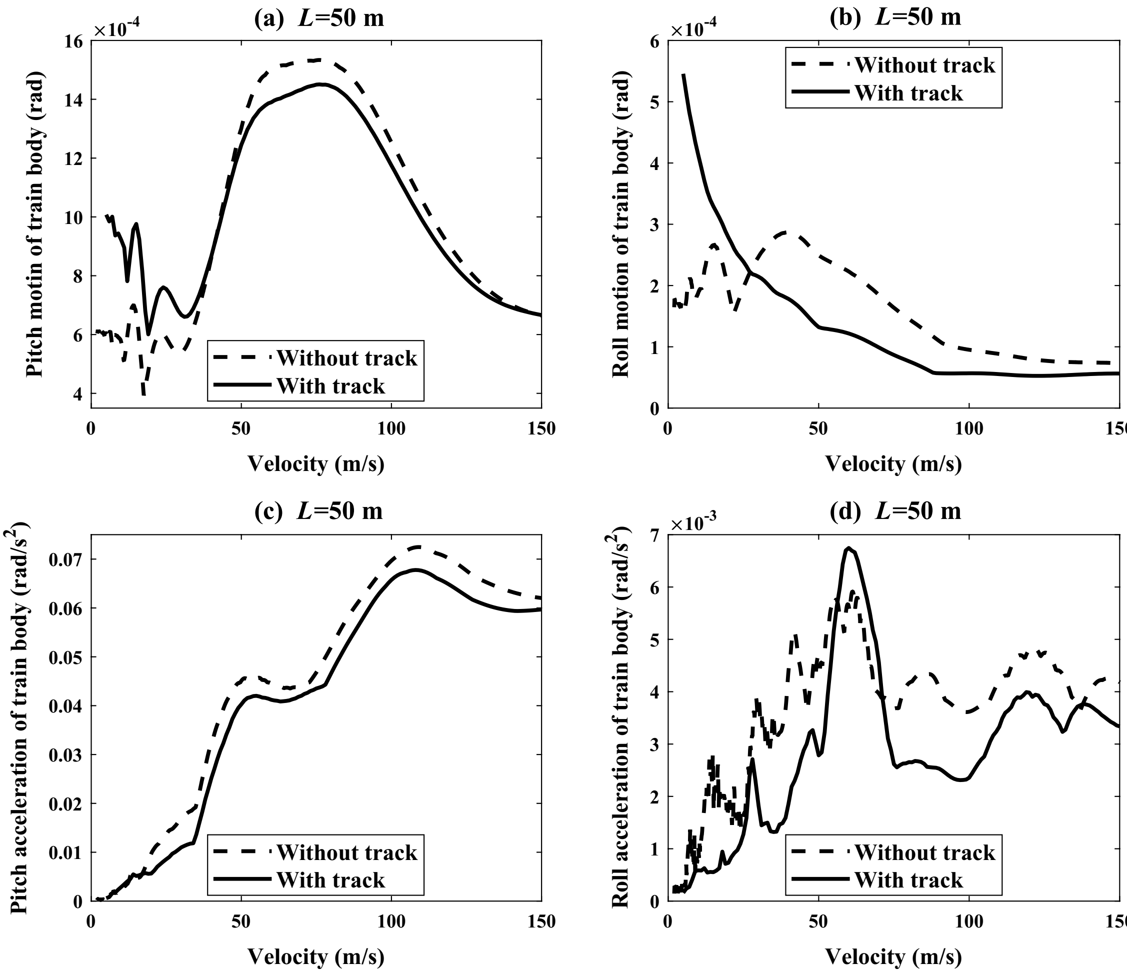

Fig. 15 Comparison of the with track and without track model results of the train body dynamic responses versus train velocity **a** pitch motion of train body, **b** roll motion of train body, **c** pitch acceleration of train body, **d** roll acceleration of train body

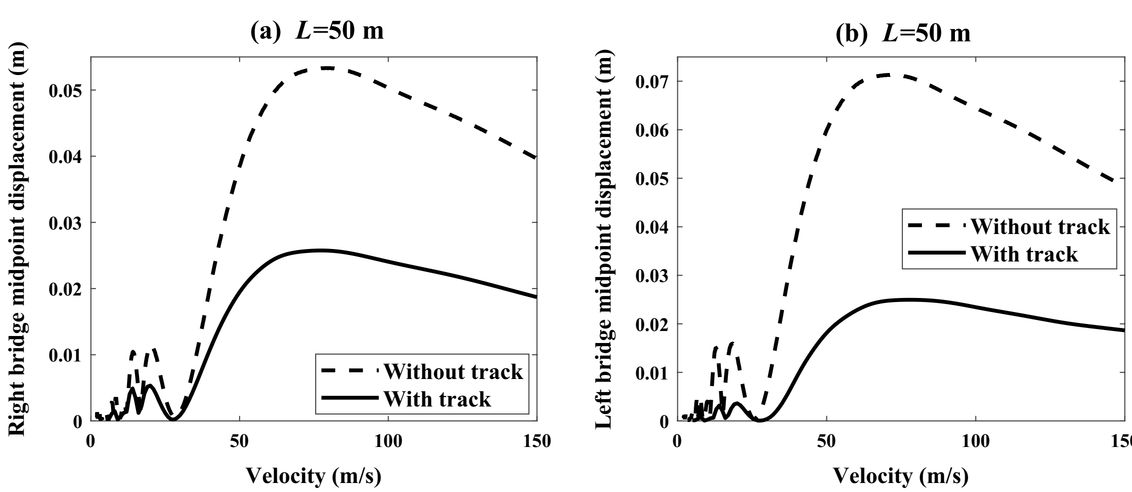

Fig. 16 Comparison of the with track and without track model results of the bridge midpoint displacement versus train velocity **a** right bridge displacement, **b** left bridge displacement

speed or at least 25% lower than the critical speed. Equation 18 [9] provides the formula for calculating the beam's natural frequency, where ω stands for the circular natural frequency of the beam.

$$\omega_j^2 = \frac{j^4\pi^4 EI}{\mu L^4}(\text{rad/s}) \tag{18}$$

In Eq. 18, the beam's circular natural frequency is given. Equation 19 determines the frequency of the beam vibration.

$$f_j = \frac{\omega_j}{2\pi} = \frac{j^2\pi}{2L^2}\sqrt{\frac{EI}{\mu}}\,(Hz) \tag{19}$$

The left and right bridge beams' first four vibration modes can be calculated using Table 5 and Eq. 19, respectively. As soon as natural frequency f_b and force frequency f_v are equal, resonance occurs. The periodic movement amplitudes rise because of the train passing over the resonance bridge. The length of the train is the most critical characteristic length for the resonance created when it crosses the beam of the bridge [89]. The critical velocity of the system is given by Eq. 20 [90].

$$V_{cr,j} = \frac{df_{b,j}}{i} \tag{20}$$

In Eq. 20, v_{cr} denotes the train's critical speed, and f_b,j is the bridge beam's natural frequency. d is the distance between the front wheel and the rear wheel. The symbol i [84, 91] denotes the number of half oscillation cycles. The symbol d is calculated as $l_{b1}+l_{b2}+l_{w1}+l_{w4}=20$ m using Table 1. As a result, the critical train speeds for the bridge's first four modes are established and are displayed in Table 5.

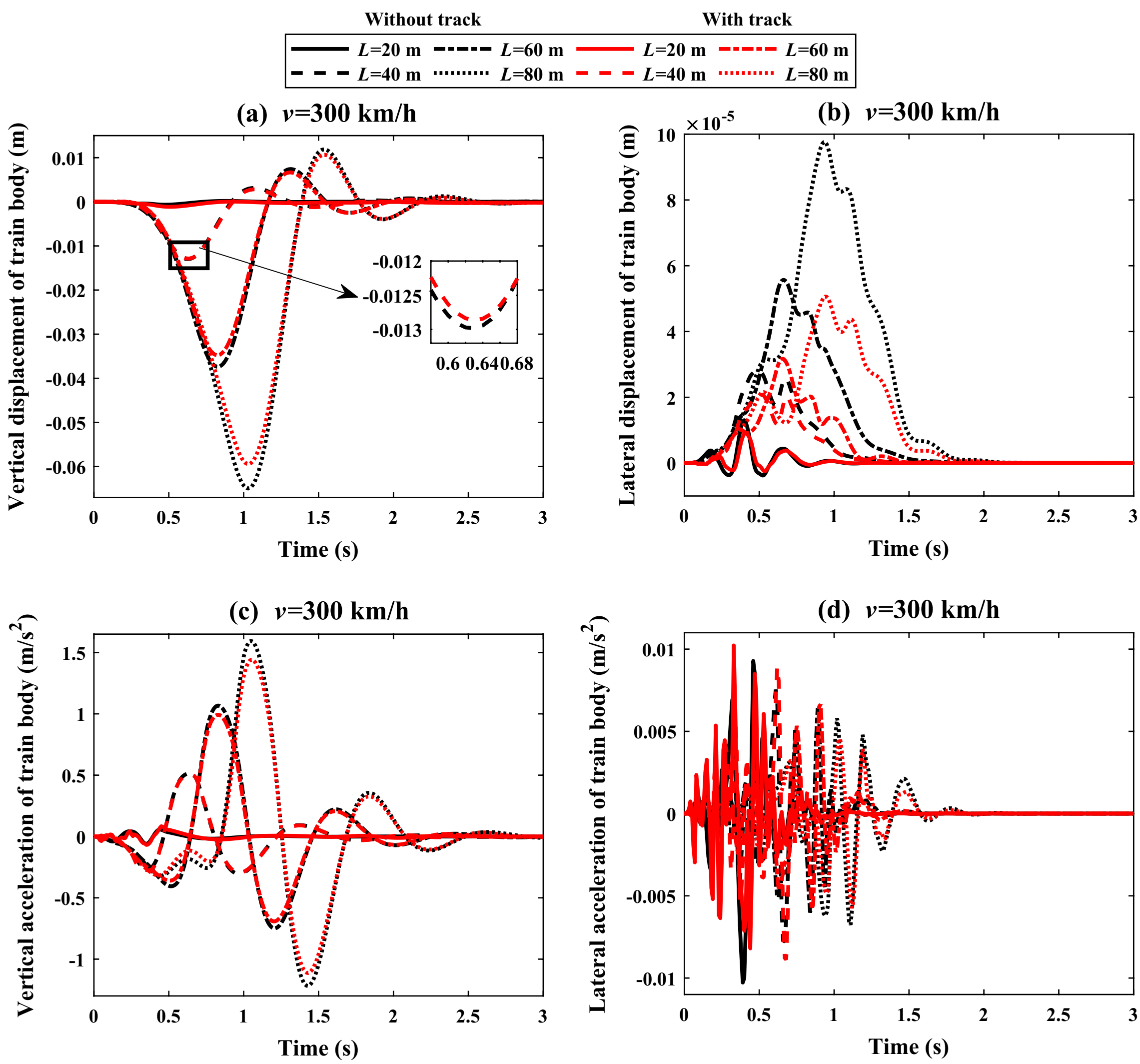

Fig. 17 Comparison of the with track and without track model results of the train body dynamic responses considering bridge length **a** vertical displacement of train body, **b** lateral displacement of train body, **c** vertical acceleration of train body, **d** lateral acceleration of train body

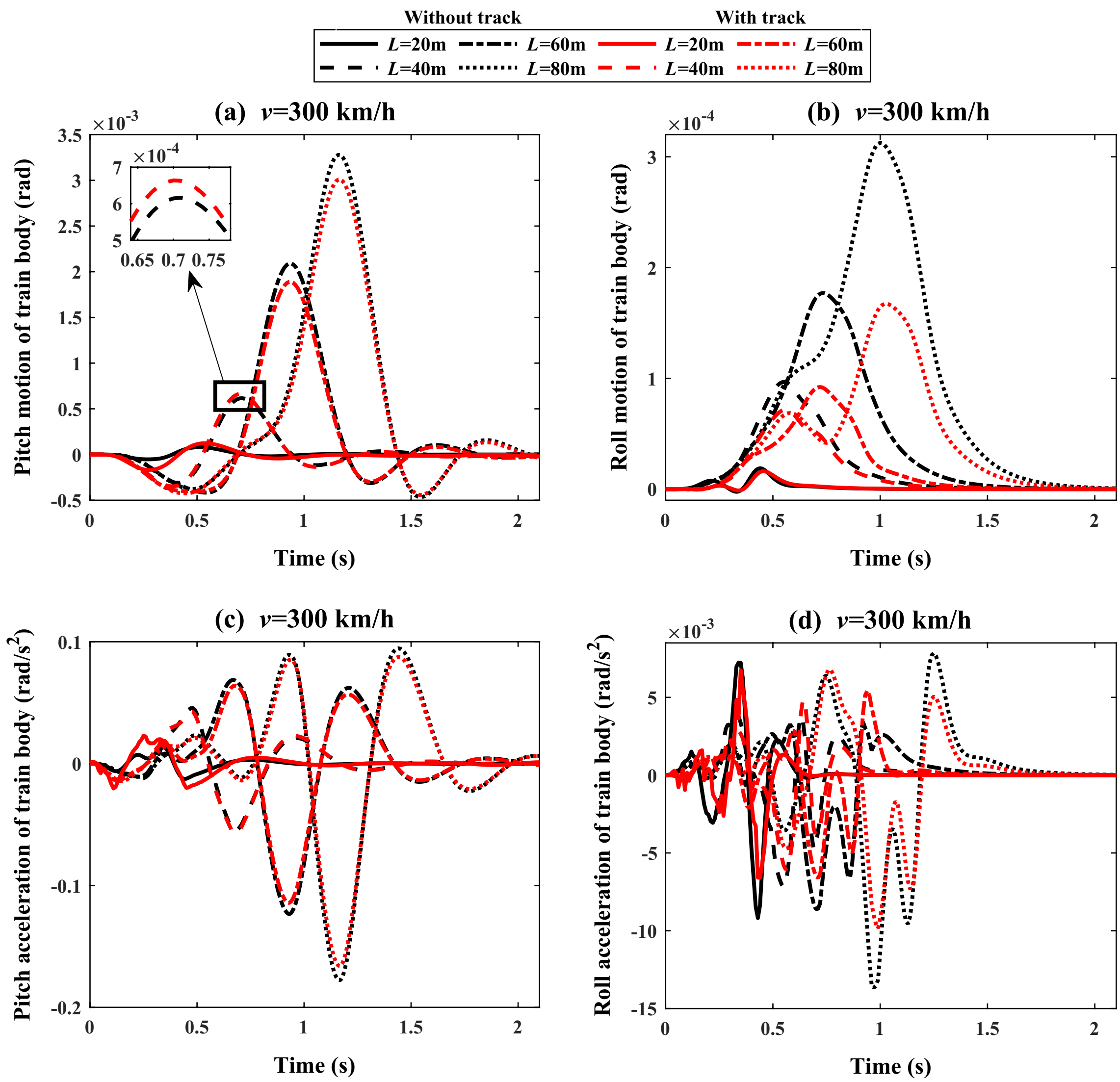

Fig. 18 Comparison of the with track and without track model results of the train body dynamic responses considering bridge length **a** pitch motion of train body, **b** roll motion of train body, **c** pitch acceleration of train body, **d** Roll acceleration of train body

In Figs. 14, 15, 16, the displacement, rotation, and acceleration of the train body and the bridge midpoint displacement are given when the train velocity changes from 2 to 150 m/s in 1 m/s interval. Examining Fig. 14, the maximum vertical displacement of the train body was nearly at 45 m/s for both models and 6.3×10^{-3} m for TBI and 5.12×10^{-3} m for TTBIS. In Fig. 13b, it is shown that the train body lateral displacement at low speeds in the TTBIS model is more than the TBI model. According to the train body's vertical acceleration in Fig. 14c, it is maximum in two places according to the results of both models. The first is 18 m/s for TBI and 20 m/s for TTBIS. Other maximum values are 69 m/s for TBI and 66 m/s for TTBIS. It is understood from Table 5 that these two maximum velocities are remarkably close to the critical velocities of the train-track-bridge systems. According to Fig. 14d, the train body lateral acceleration increases noticeably as the train velocity exceeds 90 m/s.

In Fig. 15, the train body's roll and pitch motions are given. If Fig. 15 is examined, it is shown that the pitch motion of the TTBIS model is higher when the train velocity is less than about 50 m/s, while the pitch motion of the TBI model is more when the train velocity is more than 50 m/s. The train body roll motion in Fig. 15b gave a result like the lateral displacement of the train as in Fig. 14b. If Fig. 15c, d is examined, the TTBIS model results are slightly less than the TBI model in the pitch and roll acceleration of the train body.

In Fig. 16, the displacement values of the midpoint of the bridge beams are given. In Fig. 16a, it is shown that the maximum displacement of the bridge for both models is

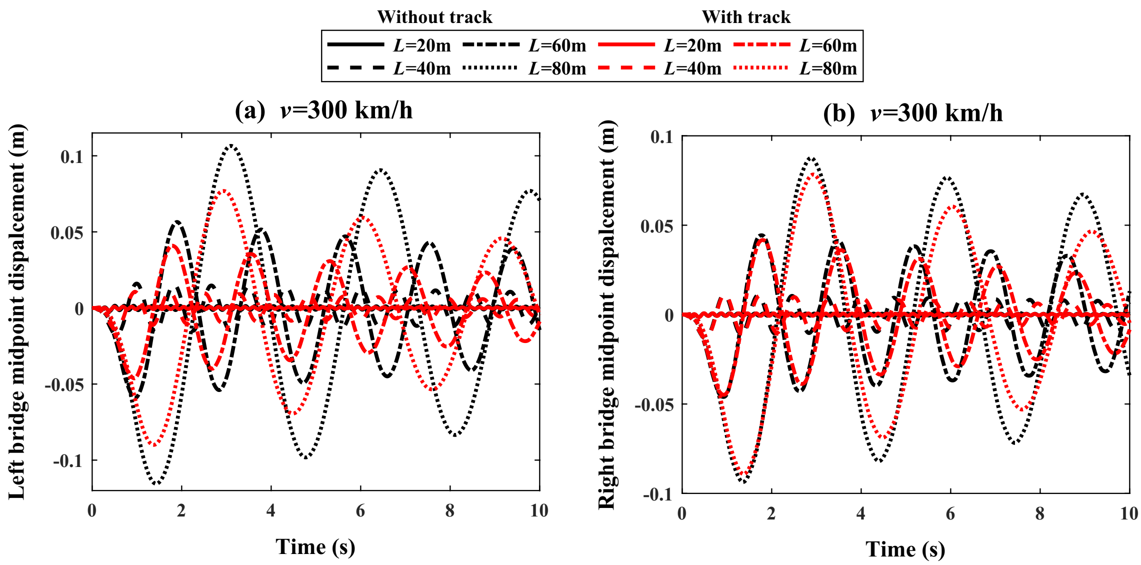

Fig. 19 Comparison of the with track and without track model results of the bridge midpoint displacement considering bridge length, **a** right bridge midpoint displacement, **b** left bridge midpoint displacement

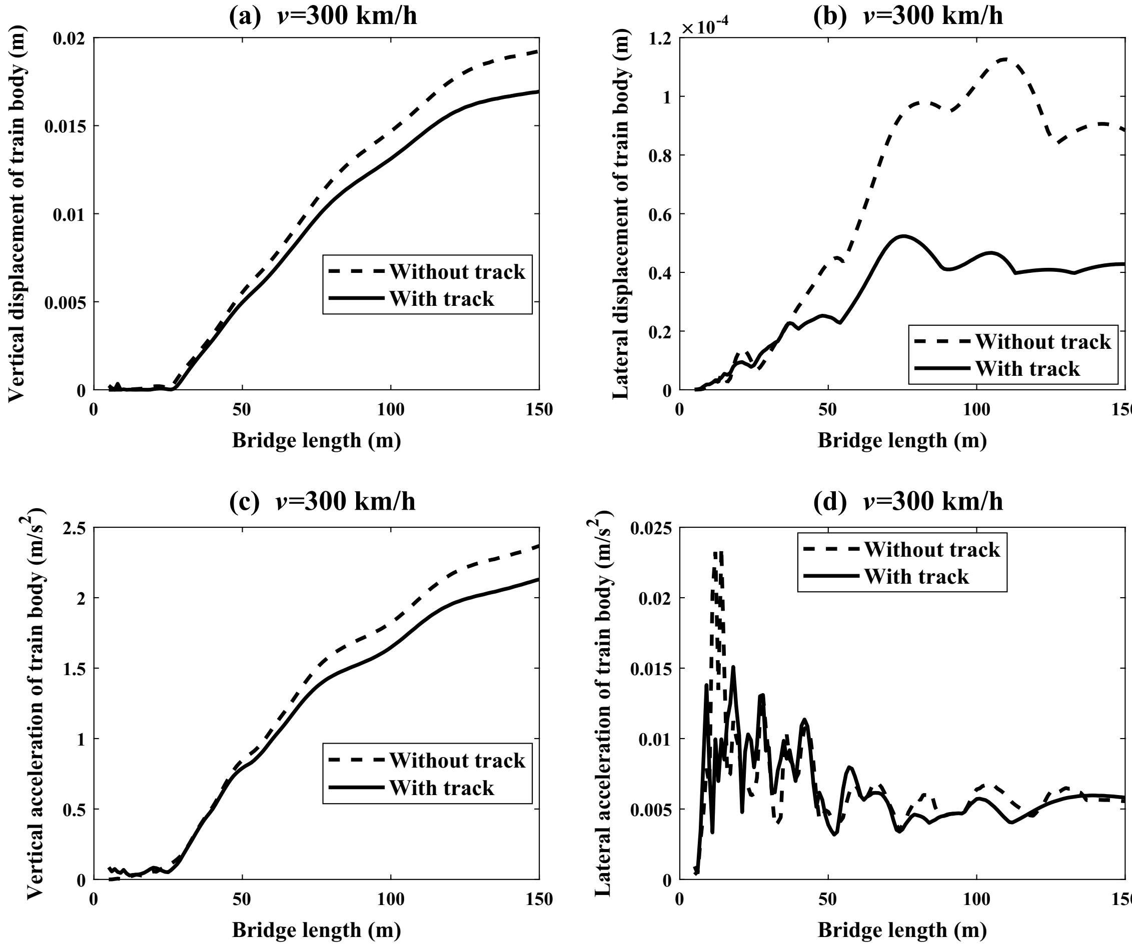

Fig. 20 Comparison of the with track and without track model results of the train body dynamic responses versus bridge length **a** vertical displacement of train body, **b** lateral displacement of train body, **c** vertical acceleration of train body, **d** lateral acceleration of train body

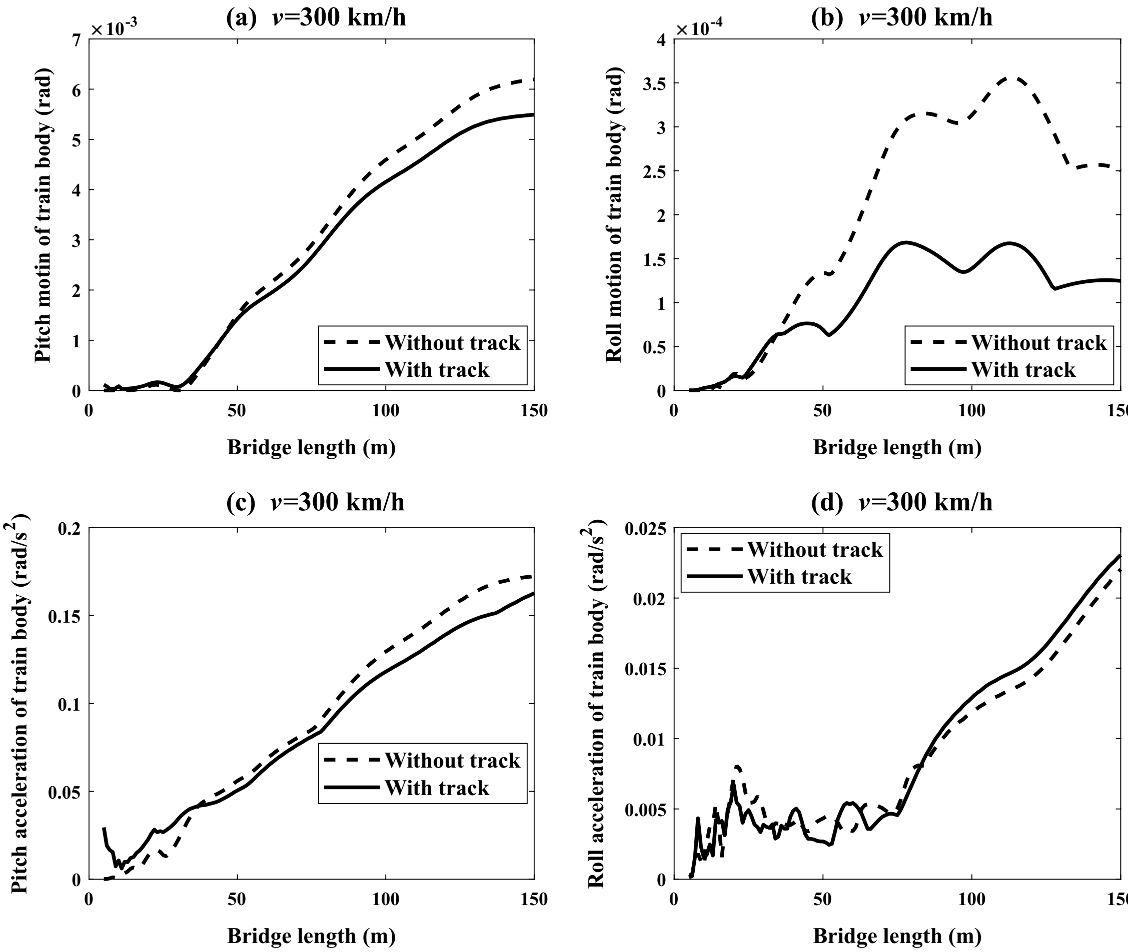

Fig. 21 Comparison of the with track and without track model results of the train body dynamic responses versus bridge length **a** pitch motion of train body, **b** roll motion of train body, **c** pitch acceleration of train body, **d** roll acceleration of train body

at the train velocities of approximately 20 m/s and 75 m/s. These two numbers are extremely close to the train-track-bridge coupled system's critical velocities. In addition, if the graph is scrutinized, the maximum deflection of the bridge beam is 0.025 m in the TTBIS model, while it is 0.053 m for the TBI model. In Figs. 17, 18, 19, the effects of four different bridge lengths as $L = 20$ m, $L = 40$ m, $L = 60$ m, and $L = 80$ m on the displacement, rotation, and acceleration of the train body have been investigated. In Fig. 17a, the maximum train body vertical displacement is given by comparing both models in the case of different bridge lengths. For four different bridges, the maximum train body vertical displacement is 0.001 m, 0.013 m, 0.037 m, and 0.06 m at times of 0.5 s, 0.63 s, 0.82 s, and 1.03 s, respectively. Similarly, the lateral displacement of the train body according to different bridge lengths is given in Fig. 17b. While the peaking times of the vertical and lateral displacements of the train body are almost the same in both graphs, the peaking times of these displacement values are distinct in models with different bridge lengths. The reason for this is related to the natural frequencies and bridge parameters that the train passes over.

The train body's vertical and lateral acceleration are given in Fig. 17c, d, respectively. In Fig. 18, the train body rotation and angular acceleration are compared using both models examined in this study. Also, in Fig. 19, the displacement of the bridge's midpoint modelled according to the Euler–Bernoulli beam theorem is given for TBI and TTBIS models. It is understood from these graphs that the dynamic responses affecting the train in long-span bridges in the TTBIS model are different compared to the TBI model. In other words, the effects on trains passing over short-span bridges are almost the same in both TBI and TTBIS models. According to these results, the use of track structure can be neglected where there are short-span bridges.

In Figs. 20, 21, dynamic responses of the train body are examined according to the length of the bridge, which varies from 5 to 150 m at 1 m intervals. While in Fig. 20a–c, the maximum vertical displacement of the train body rises with the bridge length being approximately 26 m, in Fig. 20b,

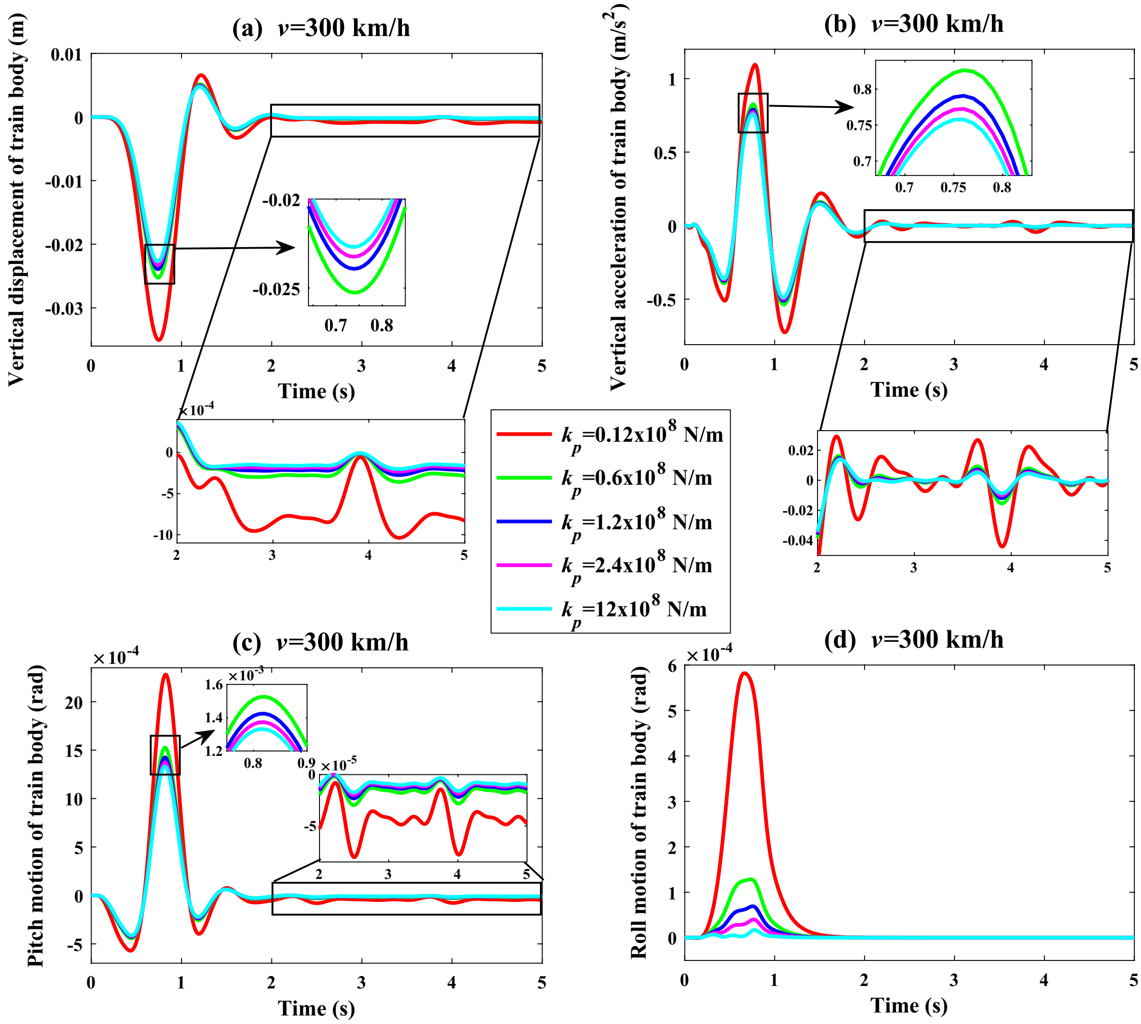

Fig. 22 Time histories of the train body's dynamic responses considering the different stiffness coefficient of railpad **a** vertical displacement of train body, **b** lateral displacement of train body, **c** vertical acceleration of train body, **d** lateral acceleration of train body

the lateral displacement values increase continuously until the bridge length is 75 m and remain almost the same after this value. In Fig. 20d, the lateral acceleration values of the train body are higher in short-span bridges, and the lateral acceleration values gradually decrease as the bridge length increases. In Fig. 21, the pitch and roll motion of the train body are almost like the graphs in Fig. 20, but only the train body roll acceleration increases when the bridge length is 75 m and longer.

Effects of Track Parameters on High-Speed Train Dynamic Response

Comparative graphics of TTBIS and TBI models are given in the previous sections of this study. The results obtained from the graphics show that the track structure generally reduces the displacements on the train body. In this section, the effect of track parameters, which is the sub-model of the TTBIS model, on the dynamic responses of the train body will be examined. In Sect. "Motion equations of the track-bridge subsystem", the introduction of the parameters in the track system and Table 3 provides these parameters' values.

In Fig. 22, the vertical and rotation motion of the train body for the different stiffness coefficients of the rubber pad between the rail and the sleeper was examined in time history. Here, the stiffness coefficient of the rubber pad is taken as 0.1, 0.5, 1, 2, and 10 times the $k_p = 1.2 \times 10^8$ N/m value given in Table 3, respectively, and a total of 5 different k_p values are defined and analysed. When Fig. 22a is examined, the maximum vertical displacement value of the train body is 0.035 m in the case of the rubber pad of $0.1k_p$, while it is almost 0.024 m for the rubber pads with other stiffness coefficients. In Fig. 22b, vertical acceleration values of the train body for five different rubber pad stiffness are given. If the stiffness coefficient of the rubber pad is $0.1 \times k_p$, the maximum train body vertical acceleration is 1.1 m/s^2, while

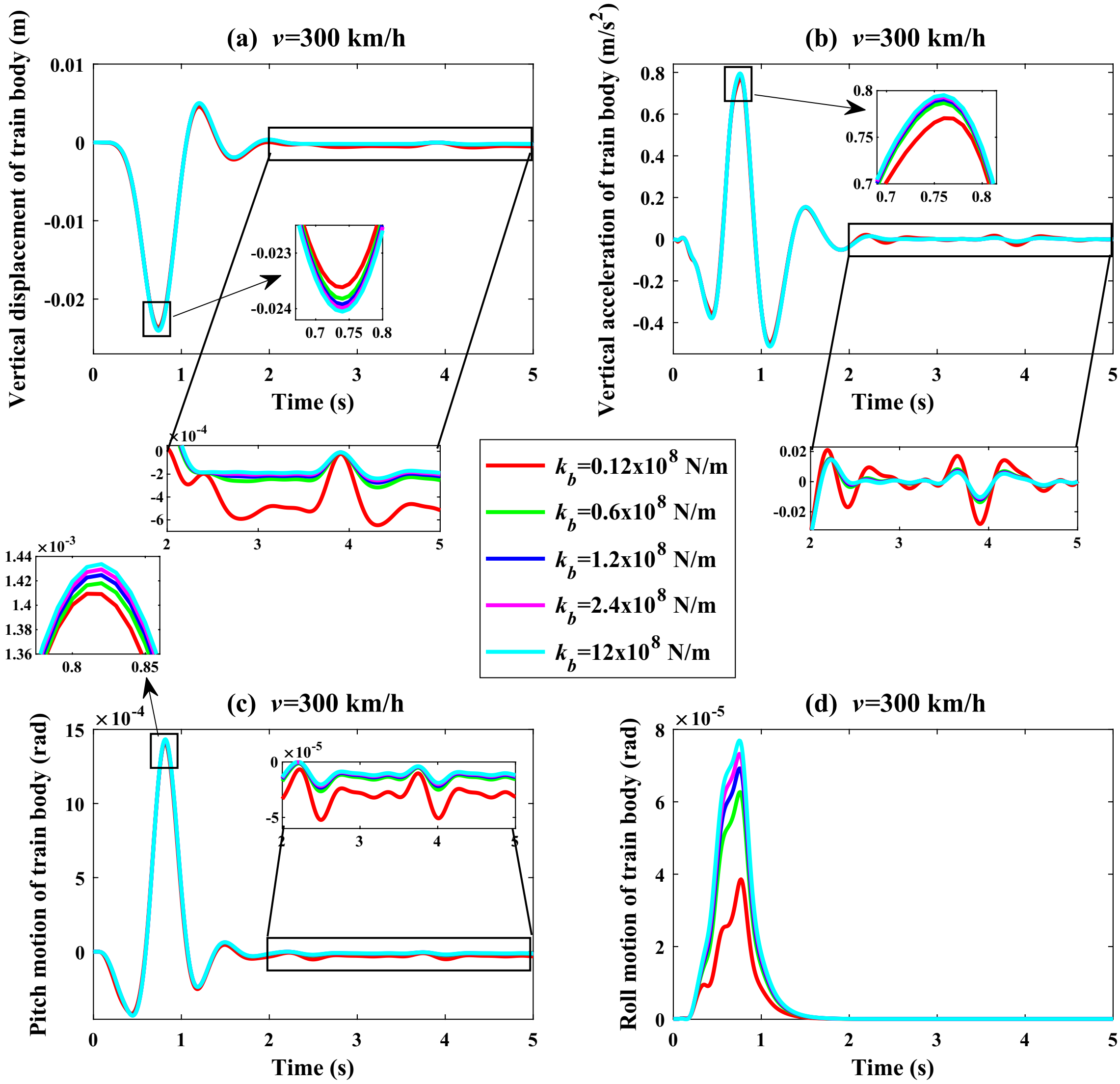

Fig. 23 Time histories of the train body's dynamic responses considering the different stiffness coefficient of ballast **a** vertical displacement of train body, **b** lateral displacement of train body, **c** vertical acceleration of train body, **d** lateral acceleration of train body

in the case of other stiffness coefficients, it is about 0.8 m/s^2. In addition, when the train passes over the track structure, the soft track structure causes more deflection values. In Fig. 22, it is seen that vertical displacements cannot be fully damped in the case of a soft rubber pad, as the train only runs on the track after 2 s of the analysis time.

In Fig. 22c, d, the train body's pitch and roll motion for a track with five different rubber pad stiffness coefficients is provided. When the graphs are examined, it is shown that the maximum value of the pitch and roll motion is high in the case of the soft rubber pad compared to the others. In addition, in the case of the soft stiffness coefficient, it is shown that the roll motion is 5–6 times higher than the other k_p values.

In Fig. 23, the train body's dynamic response is examined when the stiffness coefficient of the ballast, which is a part of the track structure, is taken at different values. In Table 3, the stiffness coefficient of the ballast is 0.1, 0.5, 1, 2, and 10 times the $k_b = 2.4 \times 10^8$ N/m value, respectively, and a total of 5 different k_b values are defined and analysed. When Fig. 23a, b is examined, it is shown that the maximum vertical acceleration and displacement value of the train is almost the same value at any value of the ballast. When Fig. 23c, d is analysed carefully, it is shown that the roll motion is less in soft ballast value, unlike Fig. 23b.

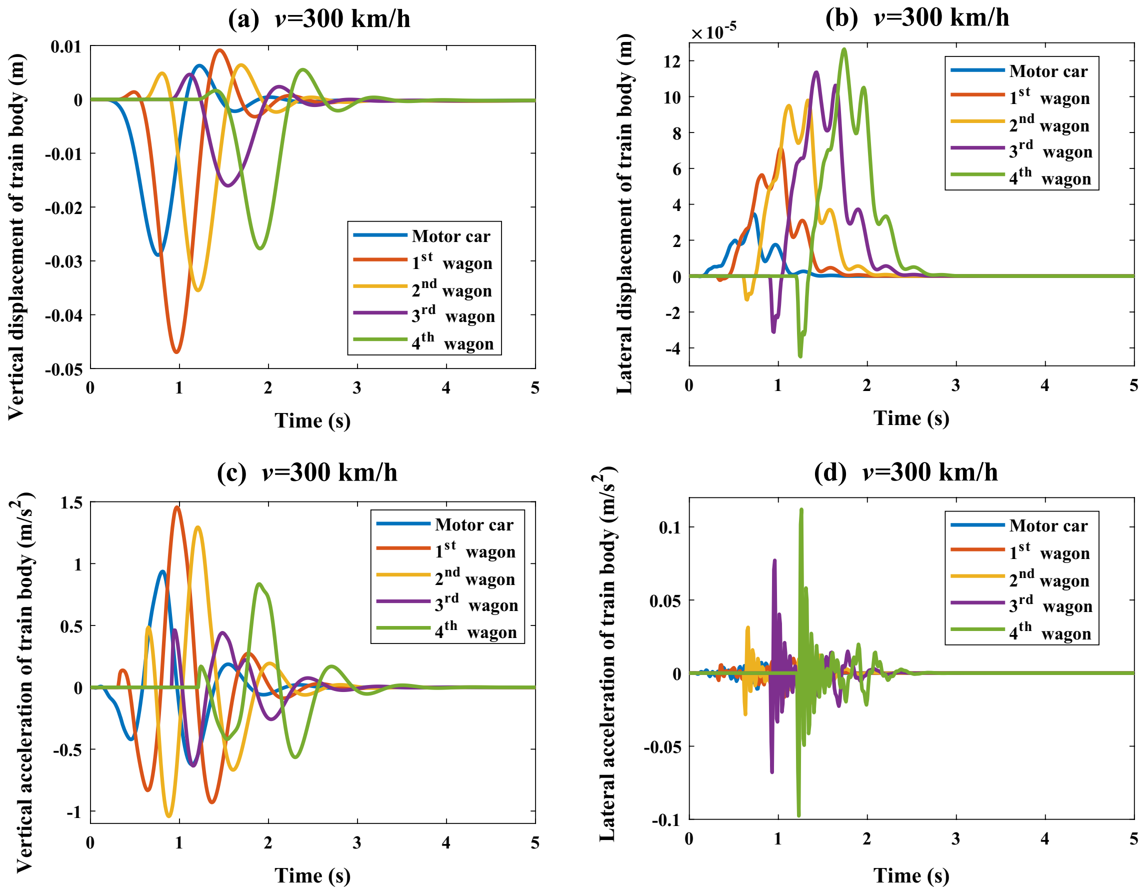

Fig. 24 Time histories of the train body's dynamic responses considering the multiple vehicles **a** vertical displacement of train body, **b** lateral displacement of train body, **c** vertical acceleration of train body, **d** lateral acceleration of train body

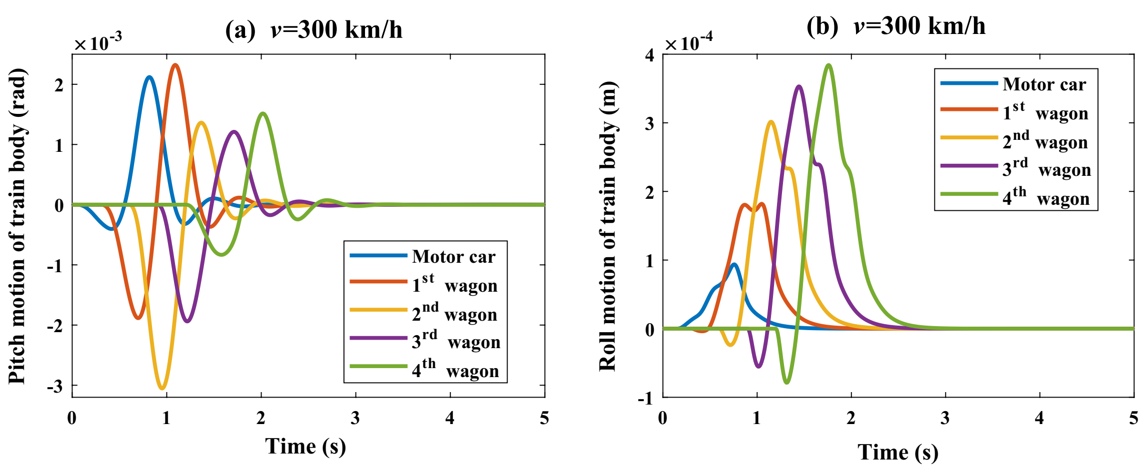

Fig. 25 Time histories of the train body's dynamic responses considering the multiple vehicles **a** pitch motion of train body, **b** roll motion of train body

Effect of Multiple Wagons Upon Dynamic Responses

In the case of more than one wagon in the TTBIS model discussed in this paper, the bridge beam's dynamic responses and the effect of these dynamic responses on each wagon were examined. Crossings multiple wagons are exemplified in Fig. 1. In Figs. 23, 24, 25, the effect of multiple wagons, each of which is the same, is given in different graphics

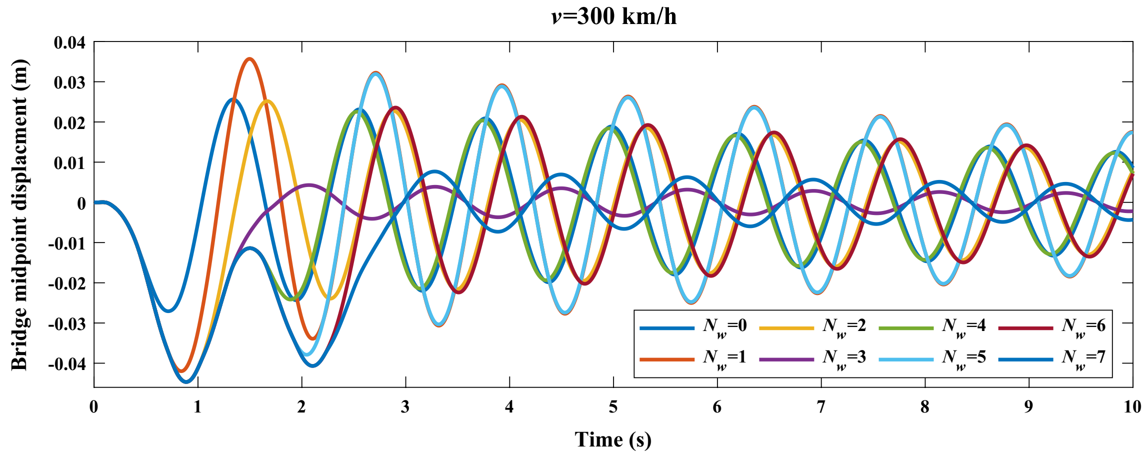

Fig. 26 Time histories of the bridge midpoint displacement considering the multiple vehicles

within the scope of TTBIS analysis. The degree of freedom of the entire system varies according to the number of wagons passing over the track-bridge subsystem, and each wagon adds an extra 31-DOFs to the system. The parameters of each wagon are taken as in Table 1, and the distance between the wheels of the successive wagons is 5.16 m.

In Fig. 24, vertical and lateral displacement and acceleration values of four wagons together with the motor car are given. When Fig. 24a is examined, the maximum vertical displacement of the motor car was found as 0.75 s at 0.029 m. Besides, the first four wagon's maximum displacements were 0.047 m, 0.035 m, 0.016 m, and 0.028 m at 0.97 s, 1.21 s, 1.55 s, and 1.9 s, respectively. The lateral distance between the midpoints of the successive wagons is $(l_{b1}+l_{b2}+2l_w+5.16)$ 25.16 m, and the difference in the maximum vertical displacement times of the wagons is due to this distance. Another remarkable situation in Fig. 24a is that the vertical displacement of the third wagon is lower than the others. An analogous situation is seen in the vertical acceleration of the wagon in Fig. 24c. In Fig. 24b–d, the train body's lateral displacement and acceleration increase as the number of wagons increases.

In Fig. 25, the train body's pitch and roll motion are given in case there are four identical wagons together with the motor car. In Fig. 26, the displacement of the bridge midpoint with respect to time is given according to the number of wagons (N_w = 0–7). When Fig. 26 is examined carefully, the minimum displacement value of the bridge midpoint occurs when the number of wagons is three and seven. In other words, if we consider the motor car as a wagon, the oscillations of the bridge in every four wagons are minimal. In addition, the effect of this situation on the train body is seen in Fig. 24. As it will be remembered, in Fig. 24, if the number of wagons was four together with the motor car, the maximum displacement of the train body was extremely low. It is understood from this that there is a relationship between bridge oscillations and the number of wagons and bridge resonance excited by the loading rate of the moving load series of wagons.

Conclusions

In this paper, the vibrations of the 31-DOFs full train model and the bridge beam with the track, which can be modelled according to the simply supported Euler–Bernoulli beam model theorem, are investigated in a comprehensive framework, taking into account the train speed, bridge beam length, track parameters and a number of wagons. It is seen from the analysis results that the train dynamic response in the vertical direction and especially in the lateral direction decreases in the presence of a track. In addition, the bridge midpoint displacement in the with track model is less than in the without track model. When different bridge lengths are considered in the comparison of with track and without track models, it is seen that as the bridge length increases, the difference in the results of the with track and without track models also increases. In other words, it is understood that if the length of the bridge is short in high-speed trains, the use of the track can be neglected. This situation is clearly seen in the presented graphs, and the results are almost similar if the bridge length of both models is approximately 50 m or less. In addition, in this study, the effect of track parameters on the dynamic response of the train has been examined. Suppose the stiffness coefficient of the rubber pad between the rail and the sleeper is taken as 10% of the best value. In that case, the vertical and lateral displacements of the train body and the pitch and roll motions increase considerably. On the other hand, when the best value is taken ten times, these values almost do not change. In addition, if there is a soft spring coefficient in the track parameters, the train oscillations are damped much later after the train passes through the bridge. Passenger-carrying high-speed trains usually do not consist of just a wagon. In other words, it consists of several wagons with the motor car. In this case, it would be unrealistic to examine only the dynamic responses of a wagon. In this study, any number of wagons can be examined in TTBIS software simulation, and the desired dynamic response of any wagon can be decided. According to the train-track-bridge system parameters used in this model, the dynamic responses of the first wagon were higher than the others. The wagon with the minor dynamic responses is the third wagon after the motor car. In addition, if there are four or eight wagons with the motor car, the displacement of the midpoint of the bridge decreases a lot. These results show a resonance mechanism connection between the bridge dynamics and the number of wagons of the high-speed train passing through the track-bridge couple subsystem. It is understood that the resonance vibrations of the train-track-bridge system depend on the periodic loading of the wheel spaces of the moving vehicles and are variable according to the parameters of the track-bridge couple subsystem.

According to the results obtained in the study, the dynamic behavior of high-speed trains varies according to the mechanical properties of the railway line. In addition, the critical speed of the train-structure is determined according to these characteristics of the railway line, and it is seen that the maximum dynamic responses of the train occur at these critical speeds. Moreover, not only the mechanical properties of the railway line change the critical speed but also the number of wagons passing over the structure. As a matter of fact, if more than one wagon crosses the bridge, the dynamic displacements of the bridge change considerably.

As a result of the study, the effect of the track of the structure where high-speed trains pass, and the dynamic interaction between the train-structure passing over this structure have been examined and it has been understood that the train and the structure affect each other. It has been understood that the resonance mechanism is particularly important in this regard, and it is crucial to develop such software programs and make such analyzes easily and cheaply in advance.

Appendix A

Using the variables in Appendix A, second-order equations have been changed into first-order equations.

$$
\begin{array}{llll}
x_1 = r_{cy} \gg \dot{x}_1 = \dot{r}_{cy} = x_2 & x_{19} = \theta_{b1y} \gg \dot{x}_{19} = \dot{\theta}_{b1y} = x_{20} & x_{37} = \theta_{w1y} \gg \dot{x}_{37} = \dot{\theta}_{w1y} = x_{38} & x_{55} = r_{w4y} \gg \dot{x}_{55} = \dot{r}_{w4y} = x_{56} \\
x_2 = \dot{r}_{cy} \gg \dot{x}_2 = \ddot{r}_{cy} & x_{20} = \dot{\theta}_{b1y} \gg \dot{x}_{20} = \ddot{\theta}_{b1y} & x_{38} = \dot{\theta}_{w1y} \gg \dot{x}_{38} = \ddot{\theta}_{w1y} & x_{56} = \dot{r}_{w4y} \gg \dot{x}_{56} = \ddot{r}_{w4y} \\
x_3 = r_{cz} \gg \dot{x}_3 = \dot{r}_{cz} = x_4 & x_{21} = r_{b2y} \gg \dot{x}_{21} = \dot{r}_{b2y} = x_{22} & x_{39} = r_{w2y} \gg \dot{x}_{39} = \dot{r}_{w2y} = x_{40} & x_{57} = r_{w4z} \gg \dot{x}_{57} = \dot{r}_{w4z} = x_{58} \\
x_4 = \dot{r}_{cz} \gg \dot{x}_4 = \ddot{r}_{cz} & x_{22} = \dot{r}_{b2y} \gg \dot{x}_{22} = \ddot{r}_{b2y} & x_{40} = \dot{r}_{w2y} \gg \dot{x}_{40} = \ddot{r}_{w2y} & x_{58} = \dot{r}_{w4z} \gg \dot{x}_{58} = \ddot{r}_{w4z} \\
x_5 = \theta_{cz} \gg \dot{x}_5 = \dot{\theta}_{cz} = x_6 & x_{23} = r_{b2z} \gg \dot{x}_{23} = \dot{r}_{b2z} = x_{24} & x_{41} = r_{w2z} \gg \dot{x}_{41} = \dot{r}_{w2z} = x_{42} & x_{59} = \theta_{w4x} \gg \dot{x}_{59} = \dot{\theta}_{w4x} = x_{60} \\
x_6 = \dot{\theta}_{cz} \gg \dot{x}_6 = \ddot{\theta}_{cz} & x_{24} = \dot{r}_{b2z} \gg \dot{x}_{24} = \ddot{r}_{b2z} & x_{42} = \dot{r}_{w2z} \gg \dot{x}_{42} = \ddot{r}_{w2z} & x_{60} = \dot{\theta}_{w4x} \gg \dot{x}_{60} = \ddot{\theta}_{w4x} \\
x_7 = \theta_{cx} \gg \dot{x}_7 = \dot{\theta}_{cx} = x_8 & x_{25} = \theta_{b2z} \gg \dot{x}_{25} = \dot{\theta}_{b2z} = x_{26} & x_{43} = \theta_{w2x} \gg \dot{x}_{43} = \dot{\theta}_{w2x} = x_{44} & x_{61} = \theta_{w4y} \gg \dot{x}_{61} = \dot{\theta}_{w4y} = x_{62} \\
x_8 = \dot{\theta}_{cx} \gg \dot{x}_8 = \ddot{\theta}_{cx} & x_{26} = \dot{\theta}_{b2z} \gg \dot{x}_{26} = \ddot{\theta}_{b2z} & x_{44} = \dot{\theta}_{w2x} \gg \dot{x}_{44} = \ddot{\theta}_{w2x} & x_{62} = \dot{\theta}_{w4y} \gg \dot{x}_{62} = \ddot{\theta}_{w4y} \\
x_9 = \theta_{cy} \gg \dot{x}_9 = \dot{\theta}_{cy} = x_{10} & x_{27} = \theta_{b2x} \gg \dot{x}_{27} = \dot{\theta}_{b2x} = x_{28} & x_{45} = \theta_{w2y} \gg \dot{x}_{45} = \dot{\theta}_{w2y} = x_{46} & x_{63} = q_1 \gg \dot{x}_{63} = \dot{q}_1 = x_{64} \\
x_{10} = \dot{\theta}_{cy} \gg \dot{x}_{10} = \ddot{\theta}_{cy} & x_{28} = \dot{\theta}_{b2x} \gg \dot{x}_{28} = \ddot{\theta}_{b2x} & x_{46} = \dot{\theta}_{w2y} \gg \dot{x}_{46} = \ddot{\theta}_{w2y} & \vdots \\
x_{11} = r_{b1y} \gg \dot{x}_{11} = \dot{r}_{b1y} = x_{12} & x_{29} = \theta_{b2y} \gg \dot{x}_{29} = \dot{\theta}_{b2y} = x_{30} & x_{47} = r_{w3y} \gg \dot{x}_{47} = \dot{r}_{w3y} = x_{48} & x_{62+4n} = \dot{q}_n \gg \dot{x}_{62+4n} = \ddot{q}_n \\
x_{12} = \dot{r}_{b1y} \gg \dot{x}_{12} = \ddot{r}_{b1y} & x_{30} = \dot{\theta}_{b2y} \gg \dot{x}_{30} = \ddot{\theta}_{b2y} & x_{48} = \dot{r}_{w3y} \gg \dot{x}_{48} = \ddot{r}_{w3y} & x_{62+4n+1} = \gamma_1 \gg \dot{x}_{62+4n+1} = \dot{\gamma}_1 \\
x_{13} = r_{b1z} \gg \dot{x}_{13} = \dot{r}_{b1z} = x_{14} & x_{31} = r_{w1y} \gg \dot{x}_{31} = \dot{r}_{w1y} = x_{32} & x_{49} = r_{w3z} \gg \dot{x}_{49} = \dot{r}_{w3z} = x_{50} & \vdots \\
x_{14} = \dot{r}_{b1z} \gg \dot{x}_{14} = \ddot{r}_{b1z} & x_{32} = \dot{r}_{w1y} \gg \dot{x}_{32} = \ddot{r}_{w1y} & x_{50} = \dot{r}_{w3z} \gg \dot{x}_{50} = \ddot{r}_{w3z} & x_{62+8n} = \dot{\gamma}_n \gg \dot{x}_{62+8n} = \ddot{\gamma}_n \\
x_{15} = \theta_{b1z} \gg \dot{x}_{15} = \dot{\theta}_{b1z} = x_{16} & x_{33} = r_{w1z} \gg \dot{x}_{33} = \dot{r}_{w1z} = x_{34} & x_{51} = \theta_{w3x} \gg \dot{x}_{51} = \dot{\theta}_{w3x} = x_{52} & x_{62+8n+1} = \psi_1 \gg \dot{x}_{62+8n+1} = \dot{\psi}_1 \\
x_{16} = \dot{\theta}_{b1z} \gg \dot{x}_{16} = \ddot{\theta}_{b1z} & x_{34} = \dot{r}_{w1z} \gg \dot{x}_{34} = \ddot{r}_{w1z} & x_{52} = \dot{\theta}_{w3x} \gg \dot{x}_{52} = \ddot{\theta}_{w3x} & \vdots \\
x_{17} = \theta_{b1x} \gg \dot{x}_{17} = \dot{\theta}_{b1x} = x_{18} & x_{35} = \theta_{w1x} \gg \dot{x}_{35} = \dot{\theta}_{w1x} = x_{36} & x_{53} = \theta_{w3y} \gg \dot{x}_{53} = \dot{\theta}_{w3y} = x_{54} & x_{62+12n} = \dot{\psi}_n \gg \dot{x}_{62+12n} = \ddot{\psi}_n \\
x_{18} = \dot{\theta}_{b1x} \gg \dot{x}_{18} = \ddot{\theta}_{b1x} & x_{36} = \dot{\theta}_{w1x} \gg \dot{x}_{36} = \ddot{\theta}_{w1x} & x_{54} = \dot{\theta}_{w3y} \gg \dot{x}_{54} = \ddot{\theta}_{w3y} & x_{62+12n+1} = \phi_1 \gg \dot{x}_{62+12n+1} = \dot{\phi}_1 \\
\vdots & & & \\
x_{62+16n} = \dot{\phi}_n \gg \dot{x}_{62+16n} = \ddot{\phi}_n & & &
\end{array}
\tag{21}
$$

Equations that are written in state-space form with state variables from Eq. (21) and equation motions from other coordinates result in the following:

$$\dot{\mathbf{X}}(t) = A(t)\mathbf{X}(t) + f(t), \tag{22}$$

$$\mathbf{X}(t) = \left\{x_1\, x_2\, \dots\, x_{62+(16n-1)}\, x_{62+16n}\right\}^T, \tag{23}$$

For the differential equation system, which consists of a total of sixty-two first-order differential equations, the four repetitive coefficients of the Runge–Kutta method are written as follows:

$$\begin{aligned} & k^i_{1(1)} = f\left(t_i, x_{1(i)}, x_{2(i)}, x_{3(i)}, \dots, x_{62+16n(i)}\right), \\ & \vdots \\ & k^i_{1(62+16n)} = f\left(t_i, x_{1(i)}, x_{2(i)}, x_{3(i)}, \dots, x_{62+16n(i)}\right), \end{aligned} \tag{24}$$

$$\begin{aligned} & k^i_{2(1)} = f\left(t_i + \frac{1}{2}\Delta t, x_{1(i)} + \frac{1}{2}k^i_{1(1)}\Delta t, x_{2(i)} + \frac{1}{2}k^i_{1(2)}\Delta t, x_{3(i)} + \frac{1}{2}k^i_{1(3)}\Delta t, \dots, x_{62+16n(i)} + \frac{1}{2}k^i_{1(62+16n)}\Delta t\right), \\ & \vdots \\ & k^i_{2(62+16n)} = f\left(t_i + \frac{1}{2}\Delta t, x_{1(i)} + \frac{1}{2}k^i_{1(1)}\Delta t, x_{2(i)} + \frac{1}{2}k^i_{1(2)}\Delta t, x_{3(i)} + \frac{1}{2}k^i_{1(3)}\Delta t, .., x_{62+16n(i)} + \frac{1}{2}k^i_{1(62+16n)}\Delta t\right), \end{aligned} \tag{25}$$

$$\begin{aligned} & k^i_{3(1)} = f\left(t_i + \frac{1}{2}\Delta t, x_{1(i)} + \frac{1}{2}k^i_{2(1)}\Delta t, x_{2(i)} + \frac{1}{2}k^i_{2(2)}\Delta t, x_{3(i)} + \frac{1}{2}k^i_{2(3)}\Delta t, \dots, x_{62+16n(i)} + \frac{1}{2}k^i_{2(62+16n(i))}\Delta t\right), \\ & \vdots \\ & k^i_{3(62+16n)} = f\left(t_i + \frac{1}{2}\Delta t, x_{1(i)} + \frac{1}{2}k^i_{2(1)}\Delta t, x_{2(i)} + \frac{1}{2}k^i_{2(2)}\Delta t, x_{3(i)} + \frac{1}{2}k^i_{2(3)}\Delta t, \dots, x_{62+16n(i)} + \frac{1}{2}k^i_{2(62+16n)}\Delta t\right), \end{aligned} \tag{26}$$

$$\begin{aligned} & k^i_{4(1)} = f\left(t_i + \Delta t, x_{1(i)} + k^i_{3(1)}\Delta t, x_{2(i)} + k^i_{3(2)}\Delta t, x_{3(i)} + k^i_{3(3)}\Delta t, \dots, x_{62+16n(i)} + k^i_{3(62+16n)}\Delta t\right), \\ & \vdots \\ & k^i_{4(62+16n)} = f\left(t_i + \Delta t, x_{1(i)} + k^i_{3(1)}\Delta t, x_{2(i)} + k^i_{3(2)}\Delta t, x_{3(i)} + k^i_{3(3)}\Delta t, \dots, x_{62+16n(i)} + k^i_{3(62+16n)}\Delta t\right), \end{aligned} \tag{27}$$

$$\begin{aligned} & x_{1(i+1)} = x_{1(i)} + \frac{\Delta t}{6}\left(k^i_{1(1)} + 2k^i_{2(1)} + 2k^i_{3(1)} + k^i_{4(1)}\right) \\ & x_{2(i+1)} = x_{2(i)} + \frac{\Delta t}{6}\left(k^i_{1(2)} + 2k^i_{2(2)} + 2k^i_{3(2)} + k^i_{4(2)}\right) \\ & \vdots \\ & x_{(62+16n)(i+1)} = x_{(62+16n)(i)} + \frac{\Delta t}{6}\left(k^i_{1(62+16n)} + 2k^i_{2(62+16n)} + 2k^i_{3(62+16n)} + k^i_{4(62+16n)}\right) \end{aligned} \tag{28}$$

Declarations

Conflict of Interest The authors declare that there is no conflict of interest in the results obtained in the manuscript.

References

1. Timoshenko S (1921) On the forced vibration of bridges. Philos Mag Ser. https://doi.org/10.1080/14786442208633953
2. Fryba L (1996) Dynamics of railways bridges. Thomas Telford Publ. https://doi.org/10.1680/dorb.34716.0003
3. Tiwari V, Sharma SC, Harsha SP (2022) Ride comfort analysis of high-speed rail vehicle using laminated rubber isolator based secondary suspension. Veh Syst Dyn. https://doi.org/10.1080/00423114.2022.2131584
4. El-Sabaa FM, Amer TS, Gad HM, Bek MA (2022) Novel asymptotic solutions for the planar dynamical motion of a double-rigid-body pendulum system near resonance. vol 10. Springer Nature Singapore. https://doi.org/10.1007/s42417-022-00493-0
5. Kargarnovin MH, Younesian D, Thompson D, Jones C (2005) Ride comfort of high-speed trains travelling over railway bridges. Veh Syst Dyn 43:173–197. https://doi.org/10.1080/00423110512331335111
6. Li D, Song H, Meng G, Meng J, Chen X, Xu R et al (2022) Dynamic characteristics of wheel–rail collision vibration for high-speed train under crosswind. Veh Syst Dyn. https://doi.org/10.1080/00423114.2022.2093761
7. Liu D, Liang X, Zhou W, Zhong M, Lu Z (2022) Fundamental research on the dynamic safety of a high-speed train under strong wind conditions. Veh Syst Dyn. https://doi.org/10.1080/00423114.2022.2086144
8. Liu D, Li X, Mei F, Xin L, Zhou Z (2022) Effect of vertical vortex-induced vibration of bridge on railway vehicle's running

performance. Veh Syst Dyn. https://doi.org/10.1080/00423114.2022.2084120
9. Frýba L (1999) Vibration of solids and structures under moving loads. Thomas Telford House. https://doi.org/10.1007/978-94-011-9685-7
10. Esen I (2011) Dynamic response of a beam due to an accelerating moving mass using moving finite element approximation. Math Comput Appl 16:171–182. https://doi.org/10.3390/mca16010171
11. Koloušek V, McLean RFFJ (1973) Dynamics in engineering structures. Butter- worths, London
12. Yang YB, Yau JD, Wu YS (2004) Vehicle–bridge ınteraction dynamics: with applications to high-speed railways.https://doi.org/10.1142/5541
13. Wu J, Dai C (1987) Dynamic responses of multispan nonuniform beam due to moving loads. J Struct Eng 113:458–474. https://doi.org/10.1061/(asce)0733-9445(1987)113:3(458)
14. Dugush YA, Eisenberger M (2002) Vibrations of non-uniform continuous beams under moving loads. J Sound Vib 254:911–926. https://doi.org/10.1006/jsvi.2001.4135
15. Jiang L, Liu C, Peng L, Yan J, Xiang P (2021) Dynamic analysis of multi-layer beam structure of rail track system under a moving load based on mode decomposition. J Vib Eng Technol 9:1463–1481. https://doi.org/10.1007/s42417-021-00308-8
16. Esen I (2013) A new finite element for transverse vibration of rectangular thin plates under a moving mass. Finite Elem Anal Des 66:26–35. https://doi.org/10.1016/j.finel.2012.11.005
17. Esen I (2019) Dynamic response of a functionally graded Timoshenko beam on two-parameter elastic foundations due to a variable velocity moving mass. Int J Mech Sci 153–154:21–35. https://doi.org/10.1016/j.ijmecsci.2019.01.033
18. Esen I (2019) A solids dynamic response of functional graded Timoshenko beams in a thermal environment subjected to an accelerating load. Eur J Mech A Solids 78:103841. https://doi.org/10.1016/j.euromechsol.2019.103841
19. Esen I (2020) Response of a micro-capillary system exposed to a moving mass in magnetic field using nonlocal strain gradient theory. Int J Mech Sci 188:105937. https://doi.org/10.1016/j.ijmecsci.2020.105937
20. Wu JJ (2005) Dynamic analysis of an inclined beam due to moving loads. J Sound Vib 288:107–131. https://doi.org/10.1016/j.jsv.2004.12.020
21. Wu JJ (2008) Transverse and longitudinal vibrations of a frame structure due to a moving trolley and the hoisted object using moving finite element. Int J Mech Sci 50:613–625. https://doi.org/10.1016/j.ijmecsci.2008.02.001
22. Michaltsos GT (2001) The influence of centripetal and Coriolis forces on the dynamic response of light bridges under moving vehicles. J Sound Vib 7:315–326. https://doi.org/10.1006/jsvi.2001.3729
23. Chang CC, Wang YM (2007) The dynamics and control of an moving mass traveling on an initially curved beam. J Mar Sci Technol 15:273–277. https://doi.org/10.51400/2709-6998.2043
24. Stanišić MM, Hardin JC (1969) On the response of beams to an arbitrary number of concentrated moving masses. J Franklin Inst 287:115–123. https://doi.org/10.1016/0016-0032(69)90120-3
25. Ting EC, Genin J, Ginsberg JH (1974) A general algorithm for moving mass problems. J Sound Vib 33:49–58. https://doi.org/10.1016/S0022-460X(74)80072-6
26. Akin JE, Mofid M (1989) Numerical solution for response of beams with moving mass. Manager 115:1–2. https://doi.org/10.1061/(ASCE)0733-9445(1989)115:1(120)
27. Biggs JM (1964) Introduction to structural dynamics. McGraw-Hill, New York
28. Wen RK (1960) Dynamic response of beams traversed by two-axle loads. J Eng Mech Div 86:91–111
29. Diana G, Cheli F (1989) Dynamic interaction of railway systems with large bridges. Veh Syst Dyn 53:37–41. https://doi.org/10.1080/00423118908968915
30. Koç MA, Esen İ, Eroğlu M, Çay Y (2021) A new numerical method for analysing the interaction of a bridge structure and travelling cars due to multiple high-speed trains. Int J Heavy Veh Syst. https://doi.org/10.1504/IJHVS.2021.114415
31. Zhai W, Han Z, Chen Z, Ling L, Zhu S (2019) Train–track–bridge dynamic interaction: a state-of-the-art review. Veh Syst Dyn 57:984–1027. https://doi.org/10.1080/00423114.2019.1605085
32. Chen Z, Fang H (2019) An alternative solution of train-track dynamic ınteraction. Shock Vib. https://doi.org/10.1155/2019/1859261
33. Cheung YK, Au FTK, Zheng DY, Cheng YS (1999) Vibration of multi-span non-uniform bridges under moving vehicles and trains by using modified beam vibration functions. J Sound Vib 228:611–628. https://doi.org/10.1006/jsvi.1999.2423
34. Stollwitzer A, Bettinelli L, Fink J (2023) The longitudinal track-bridge interaction of ballasted track in railway bridges: experimental determination of dynamic stiffness and damping characteristics. Eng Struct 274:115115. https://doi.org/10.1016/j.engstruct.2022.115115
35. Lou P, Yu ZW, Au FTK (2012) Rail-bridge coupling element of unequal lengths for analysing train-track-bridge interaction systems. Appl Math Model 36:1395–1414. https://doi.org/10.1016/j.apm.2011.08.041
36. Kohl AM, Clement K, Schneider J, Firus A, Lombaert G (2023) An investigation of dynamic vehicle-bridge interaction effects based on a comprehensive set of trains and bridges. Eng Struct. https://doi.org/10.1016/j.engstruct.2022.115555
37. König P, Salcher P, Adam C (2022) An efficient model for the dynamic vehicle-track-bridge-soil interaction system. Eng Struct. https://doi.org/10.1016/j.engstruct.2021.113769
38. Zhang X, Han Y, Wang L, Liu H, Cai CS. An adaptive surrogate model approach for random vibration analysis of the train–bridge system. Eng Struct 2023;278:115490. https://doi.org/10.1016/j.engstruct.2022.115490.
39. Gu G (2015) Resonance in long-span railway bridges carrying TGV trains. Comput Struct 152:185–199. https://doi.org/10.1016/j.compstruc.2015.02.002
40. Yau JD, Martínez-Rodrigo MD, Doménech A (2019) An equivalent additional damping approach to assess vehicle-bridge interaction for train-induced vibration of short-span railway bridges. Eng Struct 188:469–479. https://doi.org/10.1016/j.engstruct.2019.01.144
41. Ju S-H (2011) Vibration analysis of 3D timoshenko beams subjected to moving vehicles. J Eng Mech 137:713–721. https://doi.org/10.1061/(asce)em.1943-7889.0000276
42. Heydari M, Ebrahimi A, Behzad M (2014) Forced vibration analysis of a Timoshenko cracked beam using a continuous model for the crack. Eng Sci Technol Int J 17:194–204. https://doi.org/10.1016/j.jestch.2014.05.003
43. Koç MA (2021) Finite element and numerical vibration analysis of a Timoshenko and Euler-Bernoulli beams traversed by a moving high-speed train. J Brazil Soc Mech Sci Eng. https://doi.org/10.1007/s40430-021-02835-7
44. Dixit A (2014) Single-beam analysis of damaged beams: comparison using Euler–Bernoulli and Timoshenko beam theory. J Sound Vib 333:4341–4353. https://doi.org/10.1016/j.jsv.2014.04.034
45. Bizimungu G, Nkundineza C (2022) Vibration responses of the railcar under rail irregularities: case of Addis Ababa light rail transit. J Vib Eng Technol. https://doi.org/10.1007/s42417-022-00766-8
46. Vesali F, Rezvani MA, Shadfar M (2023) Attuned dynamic response of double track multi-span railway bridges under the

delayed entry of a second train. J Vib Eng Technol. https://doi.org/10.1007/s42417-023-00884-x
47. Geweda AE, El-Gohary MA, El-Nabawy AM, Awad T (2017) Improvement of vehicle ride comfort using genetic algorithm optimization and PI controller. Alex Eng J 56:405–414. https://doi.org/10.1016/j.aej.2017.05.014
48. Yildirim E, Esen I (2020) Dynamic behavior and force analysis of the full vehicle model using newmark average acceleration method. Eng Technol Appl Sci Res 10:5330–5339. https://doi.org/10.48084/etasr.3335
49. Wu Y, Yang Y, Yau J (2010) Three-dimensional analysis of train-rail-bridge ınteraction problems three-dimensional analysis of train-rail-bridge. https://doi.org/10.1076/vesd.36.1.1.3567
50. Garg VK, Dukkipati RV (1984) Dynamics of railway vehicle systems. Acad Press Canada 14:245–247. https://doi.org/10.1016/0378-3804(87)90070-2
51. Abohamer MK, Awrejcewicz J, Amer TS (2023) Modeling and analysis of a piezoelectric transducer embedded in a nonlinear damped dynamical system. Nonlinear Dyn 111:8217–8234. https://doi.org/10.1007/s11071-023-08283-3
52. Tahiri M, Khamlichi A, Bezzazi M (2022) Nonlinear analysis of the ballast influence on the train-bridge resonance of a simply supported railway bridge. Structures 35:303–313. https://doi.org/10.1016/j.istruc.2021.11.020
53. Lou P (2005) A vehicle-track-bridge interaction element considering vehicle's pitching effect. Finite Elem Anal Des 41:397–427. https://doi.org/10.1016/j.finel.2004.07.004
54. Zhai W (2020) Vehicle–track coupled dynamics theory and applications. https://doi.org/10.1007/978-981-32-9283-3_4
55. Yau JD, Frýba L (2007) Response of suspended beams due to moving loads and vertical seismic ground excitations. Eng Struct 29:3255–3262. https://doi.org/10.1016/j.engstruct.2007.10.001
56. Johansson C, Pacoste C, Karoumi R (2013) Closed-form solution for the mode superposition analysis of the vibration in multi-span beam bridges caused by concentrated moving loads. Comput Struct 119:85–94. https://doi.org/10.1016/j.compstruc.2013.01.003
57. Yang SC, Hwang SH (2016) Train-track-bridge interaction by coupling direct stiffness method and mode superposition method. J Bridge Eng 21:04016058. https://doi.org/10.1061/(asce)be.1943-5592.0000852
58. Xu YL, Li Q, Wu DJ, Chen ZW (2010) Stress and acceleration analysis of coupled vehicle and long-span bridge systems using the mode superposition method. Eng Struct 32:1356–1368. https://doi.org/10.1016/j.engstruct.2010.01.013
59. Koç MA, Esen İ, Çay Y, Çerlek Ö, Asım M, Dal H et al (2017) vibration suppression of vehicle-bridge-ınteraction system using multiple tuned mass dampers, vol 2, pp 1–8
60. Amer TS, El-Sabaa FM, Zakria SK, Galal AA (2022) The stability of 3-DOF triple-rigid-body pendulum system near resonances, vol 110. Springer Netherlands. https://doi.org/10.1007/s11071-022-07722-x
61. Passino K, Yurkovich S (1998) Fuzzy control: the basics.https://doi.org/10.1109/IEMBS.2009.5332539
62. Bathe KJ, Wilson EL (1976) Numerical method in finite element analysis. Wiley. https://doi.org/10.1002/nme.1620110913
63. Newmark NM (1959) A method of computation for structural dynamics. J Eng Mech Div ASCE 85:69–94. https://doi.org/10.1061/JMCEA3.0000098
64. Mizrak C, Esen I (2015) Determining effects of wagon mass and vehicle velocity on vertical vibrations of a rail vehicle moving with a constant acceleration on a bridge using experimental and numerical methods. Shock Vib. https://doi.org/10.1155/2015/183450
65. Chen YH, Huang YH, Shih CT (2001) Response of an infinite Tomoshenko beam on a viscoelastic foundation to a harmonic moving load. J Sound Vib 241:809–824. https://doi.org/10.1006/jsvi.2000.3333
66. Li J, Law SS, Hao H (2013) Improved damage identification in bridge structures subject to moving loads: numerical and experimental studies. Int J Mech Sci 74:99–111. https://doi.org/10.1016/j.ijmecsci.2013.05.002
67. Dyniewicz B, Bajer CI, Kuttler KL, Shillor M (2019) Nonlinear analysis: real world applications vibrations of a Gao beam subjected to a moving mass. Nonlinear Anal Real World Appl 50:342–364. https://doi.org/10.1016/j.nonrwa.2019.05.007
68. Yang YB, Wu YS (2001) A versatile element for analyzing vehicle-bridge interaction response. Eng Struct 23:452–469. https://doi.org/10.1016/S0141-0296(00)00065-1
69. Youcef K, Sabiha T, El Mostafa D, Ali D, Bachir M (2013) Dynamic analysis of train-bridge system and riding comfort of trains with rail irregularities. J Mech Sci Technol 27:951–962. https://doi.org/10.1007/s12206-013-0206-8
70. Yu Z, Mao J (2017) Probability analysis of train-track-bridge interactions using a random wheel/rail contact model. Eng Struct 144:120–138. https://doi.org/10.1016/j.engstruct.2017.04.038
71. Zhu Z, Gong W, Wang L, Bai Y, Yu Z, Zhang L (2019) Efficient assessment of 3D train-track-bridge interaction combining multi-time-step method and moving track technique. Eng Struct 183:290–302. https://doi.org/10.1016/j.engstruct.2019.01.036
72. Xu L, Zhai W (2019) A three-dimensional dynamic model for train-track interactions. Appl Math Model 76:443–465. https://doi.org/10.1016/j.apm.2019.04.037
73. Zhai W, Xia H, Cai C, Gao M, Li X, Guo X et al (2013) High-speed train–track–bridge dynamic interactions—part I: theoretical model and numerical simulation. Int J Rail Transp 1:3–24. https://doi.org/10.1080/23248378.2013.791498
74. Eroğlu M, Koç MA, Esen İ, Kozan R (2022) Train-structure interaction for high-speed trains using a full 3D train model. J Brazil Soc Mech Sci Eng. https://doi.org/10.1007/s40430-021-03338-1
75. Koç MA (2021) Analytic method for vibration analysis of track structure ınduced by high- speed train. Sak Univ J Sci 25:146–155. https://doi.org/10.16984/saufenbilder.823255
76. Yau J, Yang Y, Kuo S (1999) Impact response of high speed rail bridges and riding comfort of rail cars. Eng Struct 21:836–844. https://doi.org/10.1016/S0141-0296(98)00037-6
77. Biondi B, Muscolino G, Sofi A (2005) A substructure approach for the dynamic analysis of train-track-bridge system. Comput Struct 83:2271–2281. https://doi.org/10.1016/j.compstruc.2005.03.036
78. Xu L, Zhai W (2017) Stochastic analysis model for vehicle-track coupled systems subject to earthquakes and track random irregularities. J Sound Vib 407:209–225. https://doi.org/10.1016/j.jsv.2017.06.030
79. Bian X, Jiang H, Chang C, Hu J, Chen Y (2015) Track and ground vibrations generated by high-speed train running on ballastless railway with excitation of vertical track irregularities. Soil Dyn Earthq Eng 76:29–43. https://doi.org/10.1016/j.soildyn.2015.02.009
80. Wanming Z, Zhenxing H, Xiaolin S (2010) Prediction of high-speed train induced ground vibration based on train-track-ground system model. Earthq Eng Eng Vib 9:545–554. https://doi.org/10.1007/s11803-010-0036-y
81. Zhu Z, Gong W, Wang L, Li Q, Bai Y, Yu Z et al (2018) An efficient multi-time-step method for train-track-bridge interaction. Comput Struct 196:36–48. https://doi.org/10.1016/j.compstruc.2017.11.004
82. Iwnicki S (2006) Handbook of railway vehicle dynamics. https://doi.org/10.1201/9781420004892
83. Majka M, Hartnett M (2008) Effects of speed, load and damping on the dynamic response of railway bridges and vehicles. Comput Struct 86:556–572. https://doi.org/10.1016/j.compstruc.2007.05.002

84. Museros P, Alarcón E (2005) Influence of the second bending mode on the response of high-speed bridges at resonance. J Struct Eng 131:405–415. https://doi.org/10.1061/(ASCE)0733-9445(2005)131:3(405)
85. Yang JP, Sun JY (2020) Pitching effect of a three-mass vehicle model for analyzing vehicle-bridge interaction. Eng Struct 224:111248. https://doi.org/10.1016/j.engstruct.2020.111248
86. Froio D, Rizzi E, Simões FMF, Da Costa AP (2018) Dynamics of a beam on a bilinear elastic foundation under harmonic moving load. Acta Mech 229:4141–4165. https://doi.org/10.1007/s00707-018-2213-4
87. Hilber HM, Hughes TJR, Taylor RL (1977) Improved numerical dissipation for time integration algorithms in structural dynamics. Earthq Eng Struct Dyn 5:283–292. https://doi.org/10.1002/eqe.4290050306
88. Zhu Q, Li L, Chen CJ, Liu CZ, Hu GD (2018) A low-cost lateral active suspension system of the high-speed train for ride quality based on the resonant control method. IEEE Trans Ind Electron 65:4187–4196. https://doi.org/10.1109/TIE.2017.2767547
89. Museros P (2002) Vehicle-bridge interaction and resonance effects in simply supported bridges for high speed lines. Tech Univ Madrid. https://doi.org/10.1016/S0022-460X(02)01463-3
90. Frýba L (2001) A rough assessment of railway bridges for high speed trains. Eng Struct 23:548–556. https://doi.org/10.1016/S0141-0296(00)00057-2
91. Yau JD, Yang YB (2006) Vertical accelerations of simple beams due to successive loads traveling at resonant speeds. J Sound Vib 289:210–228. https://doi.org/10.1016/j.jsv.2005.02.037